Transforming heat transfer with thermal metamaterials and devices

Ying Li[1,2,3,10], *Wei Li*[4,5,10], *Tiancheng Han*[6,10], *Xu Zheng*[7,10], *Jiaxin Li*[1,8], *Baowen Li*[7,9]✉, *Shanhui Fan*[4]✉ *and Cheng-Wei Qiu*[1]✉

Abstract | The demand for sophisticated tools and approaches in heat management and control has triggered the fast development of fields that include conductive thermal metamaterials, nanophononics, and far-field and near-field radiative thermal management. In this Review, we offer a unified perspective on the control of heat transfer, summarizing complementary paradigms towards the manipulation of physical parameters and the realization of unprecedented phenomena in heat transfer using artificial structures. The Review is divided into three parts that focus on the three main categories of heat flow control. Thermal conduction and radiation, at both the macroscale and microscale, are emphasized in the first and second parts. The third part discusses efforts to actively introduce heat sources or tune the material parameters with multiphysical effects in conduction, radiation and convection. We conclude by analysing the challenges in this research area and surveying new possible directions, in particular topological thermal effects, heat waves and quantum thermal effects.

Heat transfer is a fundamental phenomenon underpinning energy transport[1] and is generally induced by a temperature difference in space. The main concerns of heat transfer studies are temperature and heat flux management — heating or cooling targets to suitable temperatures; and energy harvesting — converting the thermal energy from a heat source (such as the Sun) to work or to other forms of energy. Today, controlling heat is particularly important to address problems such as global warming, the energy crisis and the heating of electronic devices. Alleviating these issues requires advanced tools to manipulate heat transfer in various forms at different length scales.

In recent years, developments in material science and physics have stimulated a renaissance of heat transfer research. On the one hand, new approaches with improved efficiency, accuracy, adaptiveness, tunability and compactness are emerging for the traditional purposes of heating, cooling and harvesting energy. On the other hand, new applications have been proposed that treat heat as an information carrier, and manipulate it for communication, detection, anti-detection and calculations. These advances have generated several research directions, including conductive thermal metamaterials[2,3], nanophononics[4], and far-field[5,6] and near-field[7] thermal radiation management.

In this Review, we discuss studies on various thermal metamaterials and devices in a unified framework, that of the manipulation of heat transfer through their unusual thermal conductivity and emissivity, which correspond to the two main forms of heat transfer: conduction and radiation. We also survey active approaches using material properties related to multiphysical effects. Heat transfer is a very broad topic, and here we focus on works targeted at controlling it through artificial structures and devices such as metamaterials, nanophononic crystals and systems with active sources, rather than on the study of phenomena, mechanisms, and natural or synthesized materials. Studies that aim at using heat transfer for purposes such as heat engines or thermal memories are beyond our scope, as are traditional devices such as heat sinks and heat pipes.

Heat conduction is the main form of heat transport in solids. Engineering the thermal conductivity is central to its manipulation. At the macroscale, such manipulation has been demonstrated in various conductive thermal metamaterials. An early proposal was for a thermal cloak[8,9] that was theoretically designed to render an object undetectable through temperature measurements. This was then experimentally realized with layered structures that achieved the required anisotropic thermal conductivity[10]. At the microscale, the design of thermal materials and devices is mostly based on phonon transport and scattering. Many works in the field of nanophononics[11] proposed to engineer the thermal conductivity with coherent phonon transport[12], phononic crystals[13] and local resonances[14]. In particular, advances in nonlinear phononics have made the thermal diode and thermal transistor possible, and even thermal logic gates and a thermal memory have been demonstrated[4].

✉*e-mail:*
baowen.Li@colorado.edu;
shanhui@stanford.edu;
chengwei.qiu@nus.edu.sg

https://doi.org/10.1038/s41578-021-00283-2

Thermal radiation carries heat in the form of photons or electromagnetic waves. When the distance between objects is larger than the wavelength of the thermal radiation (the thermal wavelength), the radiation is in the far-field regime. Far-field thermal radiation from high-temperature objects plays a vital role, for example, in solar energy harvesting, incandescent lighting and radiative cooling. Around room temperature, the wavelength of far-field radiation is mainly in the infrared, a spectral range that has become important in detection technologies such as night vision. Recent advances in the manipulation of far-field thermal radiation using sub-wavelength structures[15,16] have enabled phenomena that are very different from those governed by Plank's and Kirchhoff's laws, with promising applications in energy harvesting and information processing. When the distance between objects is sub-wavelength, the radiation is in the near-field regime[17], and the amount of transferred heat can be greatly enhanced compared with the far-field case[18], enabling new applications at the microscale.

The research directions above are mostly focused on developing passive approaches to controlling heat transfer. However, heat transfer can also be actively manipulated through multiphysical effects. The most common heat sources and drains are based on Joule heating and Peltier cooling. Introducing thermoelectric components with feedback enables great control over heat conduction, including apparent negative thermal conductivity, at the cost of energy input[19]. Another important application of multiphysical effects is the tailoring or tuning of material parameters such as conductivity[20] or emissivity[21] by using other physical quantities such as electric fields. Heat convection can be considered as a multiphysical effect as well, because it is coupled with the velocity field, which is a useful tool for heat transfer manipulation[22].

Manipulating heat conduction

Macroscopic approaches

Many current lines of research on the manipulation of heat conduction are based on microscopic mechanisms. At the macroscale, there are fewer degrees of freedom; thus, designing the spatial distribution of thermal conductivity (including the geometric boundaries and interfaces) constitutes the majority of present passive approaches. Conductive thermal metamaterials[2,3] (BOX 1) are artificial structures used in this context. They are often simply called thermal metamaterials, but in this Review we use this term to refer to all kinds of metamaterials for heat transfer control, including the nanophononic and photonic metamaterials that are discussed in later sections.

Transformation theory. Maxwell's equations elucidate how light propagates, and only require knowledge of the permittivity and permeability distributions in space. Transformation optics enables us to solve the inverse problem: that is, how to realize a specific light field by designing the material parameters[23,24]. It is based on the form invariance of Maxwell's equations under coordinate transformation, which ensures identical solutions in both coordinates. One can thus realize a target electromagnetic field by applying a coordinate transformation to a known solution, such as a plane wave in free space. The material parameters are derived from those of the free space in the new coordinate system. Transformation theory has been successfully applied to macroscopic heat conduction, thanks to the form invariance of the equation governing it at steady states[8,9] and transient states[25]. For a transformation from a virtual space r' to the real space r, the parameters in the two spaces are connected through the relationships[3] $\kappa = A\kappa' A^{\mathrm{T}}/\det(A)$ and $\rho c_p = \rho' c_p'/\det(A)$, where A is the Jacobian matrix for the transformation $r' \rightarrow r$, ρ is the mass density, c_p is the specific heat capacity and κ is the thermal conductivity.

One example is the thermal cloak, which prevents heat from entering the cloaking region to keep a uniform interior temperature without perturbing the exterior field. The transformation in the polar coordinate system (r,θ) is carried out along the radial direction with[25] $r = R_1 + (R_2 - R_1)r'/R_2$, where R_1 and R_2 are the interior and exterior radii of the cloak, respectively. Under this transformation, the region $(0 \le r' \le R_2)$ is squeezed into a shell $(R_1 \le r \le R_2)$, while the remaining region $(r \ge R_2)$ is unchanged. The heat flux is thus prevented from entering the cloaking region $(r \le R_1)$, while the exterior fields are undistorted. The material parameters of a cylindrical cloak are $\kappa_{rr}/\kappa_0 = \kappa_0/\kappa_{\theta\theta} = (r - R_1)/r$, $\kappa_{r\theta} = \kappa_{\theta r} = 0$ and $\rho c_p = \rho_0 c_{p0}[R_2/(R_2 - R_1)]^2(r - R_1)/r$, where κ_0, ρ_0 and c_{p0} are the thermal conductivity, density and specific heat capacity of the background, respectively.

These parameters have singularities that are difficult to realize, so reduced versions were proposed[25] with $\kappa_{rr} = \kappa_0[R_2(r - R_1)/r(R_2 - R_1)]^2$, $\kappa_{\theta\theta} = \kappa_0 R_2^2/(R_2 - R_1)^2$, $\kappa_{r\theta} = \kappa_{\theta r} = 0$ and $\rho c_p = \rho_0 c_{p0}$. The reduced thermal cloak has no singularity in κ_{rr} and has constant $\kappa_{\theta\theta}$ and ρc_p. Based on these parameters, a transformation-based thermal cloak was experimentally demonstrated[26] (FIG. 1a). For the practical realization, one needs to discretize the cloaking shell into N homogeneous layers. Then, each layer, which is homogeneous but anisotropic, can be realized by drilling holes into a copper plate and filling them with polydimethylsiloxane according to the effective medium theory[27].

Author addresses

[1]Department of Electrical and Computer Engineering, National University of Singapore, Singapore, Singapore.
[2]Interdisciplinary Center for Quantum Information, State Key Laboratory of Modern Optical Instrumentation, ZJU-Hangzhou Global Scientific and Technological Innovation Center, Zhejiang University, Hangzhou, China.
[3]International Joint Innovation Center, Key Lab. of Advanced Micro/Nano Electronic Devices & Smart Systems of Zhejiang, The Electromagnetics Academy of Zhejiang University, Zhejiang University, Haining, China.
[4]Department of Electrical Engineering, Ginzton Laboratory, Stanford University, Stanford, CA, USA.
[5]GPL, State Key Laboratory of Applied Optics, Changchun Institute of Optics, Fine Mechanics and Physics Chinese Academy of Sciences, Changchun, China.
[6]National Engineering Research Center of Electromagnetic Radiation Control Materials, State Key Laboratory of Electronic Thin Film and Integrated Devices, University of Electronic Science and Technology of China, Chengdu, China.
[7]Department of Physics, University of Colorado, Boulder, CO, USA.
[8]School of Mechatronics Engineering, Harbin Institute of Technology, Harbin, China.
[9]Paul M. Rady Department of Mechanical Engineering, University of Colorado, Boulder, CO, USA.
[10]These authors contributed equally: Ying Li, Wei Li, Tiancheng Han, Xu Zheng.

An earlier work experimentally demonstrated a multilayered thermal cloak based on only two kinds of natural bulk materials (homogeneous and isotropic)[10]. The idea is also based on transformation theory, but only engineers the thermal conductivity and works at the steady state. The realization of an ideal transformation-based thermal cloak remains challenging. Existing devices usually have good performance at the steady state, but are detectable in the transient state[28] because of their reduced density and heat capacity.

Unlike a thermal cloak, a thermal concentrator enhances its interior temperature gradient[10,25]. The corresponding transformation maps regions $R_3 \le r' \le R_2$ and $r' \le R_3$ in the virtual space to regions $R_1 \le r \le R_2$ and $r \le R_1$ (where $R_1 < R_3$), respectively. It can be realized by using two different materials aligned in the radial direction[29]. Another kind of heat collector is a thermal converging device that guides heat towards a desired spot by performing regional rotation transformations[30]. For both thermal cloaks and concentrators, the region $r \ge R_2$ is unchanged, so one can easily place multiple copies of these devices in one temperature field without interference. It has been proposed to treat the zero and enhanced temperature gradients inside these independent devices as binary digits, such that information can be encoded in the temperature field[31]. Thermal cloaking and concentrating can also be realized within a doublet thermal meta-device[32], which consists of mechanically movable blocks of two materials.

Transformation theory is also applicable to heat sources. Thermal illusion[33] is an effect in which the temperature field surrounding a heat source is modified such that a measurement of the modified field will not reveal the real shape, size or number of the heat sources. It is achieved by transforming the region occupied by the heat source into other shapes.

According to the Stefan–Boltzmann law (as discussed in the section on manipulating thermal radiation), the surface temperature field and emissivity of an object determine its thermal emission and thereby its thermal image. Therefore, one can modify the radiative signal by manipulating the heat conduction near the surface of an object. Based on this idea, a structured thermal surface has been fabricated for radiative camouflage[34,35]. Using a non-invasive transformation, the resulting device can produce arbitrary background temperature distributions on its top. When the device has similar integrated emissivity to the background (which can be easily achieved by covering it with a thin film), its image as measured by a common infrared camera is almost identical to that of a pure background. Thus, such a device can manipulate thermal radiation in complex environments. A big advantage of transformation theory is that the function of the device is independent of the temperatures of the device and background, whereas emissivity engineering usually requires such knowledge. However, the devices often have bulky and rigid metal structures, which require further optimization. The idea of using thermal conduction to manipulate the surface temperature and thereby the radiation was also demonstrated in the generation of arbitrary infrared thermograms without relying on transformation[36].

Directly solving the equation. An object can be identified through its unique scattering signature in various physical fields. Based on the scattering solutions, a direct current magnetic cloak that consists of a ferromagnetic

Box 1 | **Macroscopic heat conduction and conductive thermal metamaterials**

Heat conduction equation

Heat flows spontaneously from high-temperature regions to low-temperature regions. According to Fourier's law, macroscopic heat conduction is governed by the equation $q = -\kappa \cdot \nabla T$, where q is the heat flux density, T is temperature and κ is the thermal conductivity tensor. Taking into account energy conservation, the temperature field follows

$$\rho c_p \partial T/\partial t = \nabla \cdot (\kappa \cdot \nabla T) + g(\mathbf{r}, t) \quad (1)$$

where t is time, $\mathbf{r}$ is the position vector, $g(\mathbf{r},t)$ is the rate of energy generation, and ρ and c_p represent mass density and specific heat capacity at constant pressure, respectively. Ignoring interfacial thermal resistance[279], at the interface between two regions A and B with thermal conductivity κ_A and κ_B, the temperature (T_A, T_B) and the heat flux normal to the interface should match

$$T_A = T_B \quad (2)$$

$$-(\boldsymbol{\kappa}_A \cdot \nabla T_A) \cdot \mathbf{n} = -(\boldsymbol{\kappa}_B \cdot \nabla T_B) \cdot \mathbf{n} \quad (3)$$

where $\mathbf{n}$ is the unit vector normal to the interface. Note that at the nanoscale, the interfacial thermal resistance is non-negligible and even asymmetric, leading to an asymmetric temperature drop at the interface and thermal rectification[280]. The effect of the interfacial thermal resistance demands more attention as thermal devices reach the nanoscale. We do not have space to discuss this broad topic, which is mostly related to microscopic mechanisms; interested readers may refer to dedicated review articles[279,281–283].

Thermal conductivity

Conventional materials often have uniform and isotropic thermal conductivities ranging between ~0.03 $W m^{-1} K^{-1}$ (air, expanded polystyrene) and ~400 $W m^{-1} K^{-1}$ (copper, silver). The thermal conductivity of diamond[284] can reach ~2,000 $W m^{-1} K^{-1}$, comparable to the in-plane thermal conductivity of bulk graphite[285], but these materials are not commonly used, because of the high cost of diamond and the anisotropy of graphite. Recently, high thermal conductivities (~1,500 $W m^{-1} K^{-1}$) were reported for semiconductors such as boron arsenide[286–288] and isotope-enriched boron nitride[289]. The thermal conductivity of most natural materials is isotropic (κ is a scalar), but for single-crystalline materials such as graphite, the intrinsic orientation of the lattice can induce anisotropy. For conductive thermal metamaterials, a major advantage is that the anisotropy of their effective thermal conductivities can be engineered in a wide range by using composite structures. When the thermal conductivity is anisotropic, κ is a symmetric tensor for common materials according to the Onsager reciprocity theorem[290]. When magnetic fields are present, the effective thermal conductivity of a material can be asymmetric because of the thermal Hall effect[291].

Conductive thermal metamaterials

The temperature field is measured through various thermography techniques[292]. As an information carrier, the temperature field can also be operated for computations[4]: conductive thermal metamaterials can manipulate it with good robustness and accuracy. Conductive thermal metamaterials thus enable interesting phenomena, including the encryption[248], concealment[8,9], camouflage[33,34] and rectification[49] of heat signals measured by an infrared camera or a temperature probe. These effects have many direct and indirect applications. The camouflage of radiative signals can be directly used for infrared anti-detection. The concealment and processing of conductive heat signals are important building blocks, for example, for thermal concentrators[29], which collect heat from the environment for energy conversion. An energy-free thermostat[53] was proposed based on a thermal cloak. A modular design of thermal unit cells[55] can manage the temperature field on a circuit board. These devices offer attractive features such as low cost, adaptiveness and tunability into thermal energy utilization and temperature management, and are expected to help in realistic situations when coupled, for example, with thermoelectric modules[293] and heat sinks.

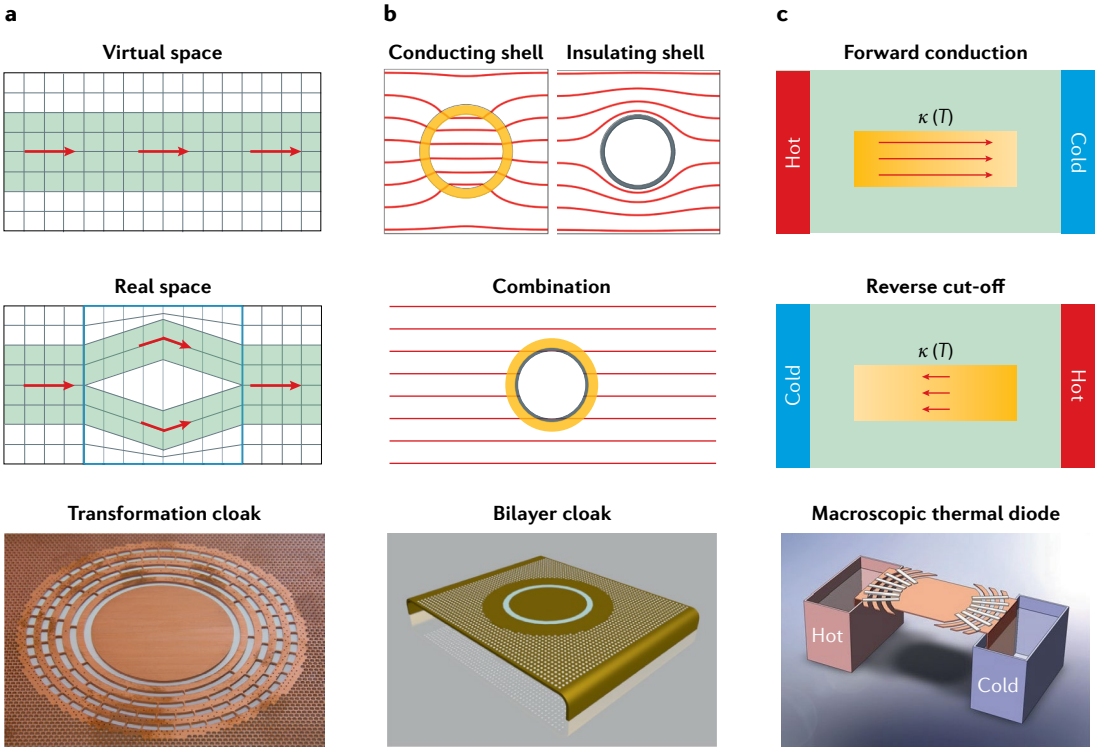

Fig. 1 | **Macroscopic approaches for manipulating heat conduction. a** | Transformation theory makes the real space equivalent to the virtual space when a specially designed thermal metamaterial fills the transformation region (blue square), providing a powerful tool for the design of transformation-based thermal cloaks[26]. The red arrows indicate the heat flow. The image shows a thermal cloak designed using transformation theory and made from layers of copper with holes filled with polydimethylsiloxane. **b** | Directly solving the thermal conduction equation enables the fabrication of a bilayer cloak that consists of an inner insulating shell and an outer conducting shell, which shields its interior from thermal radiation without distorting it[42] (red lines). The bilayer cloak is made from an inner layer of polydimethylsiloxane and an outer layer of copper. **c** | A temperature-dependent transformation enables the fabrication of devices with asymmetric behaviour of the heat current, for example a thermal diode such as the one shown in the picture, which conducts heat in one direction but insulates heat in the opposite direction[49]. The thermal diode is made from copper (orange) and bimetallic strips of shape-memory alloys and copper (white). Panel **a** reprinted with permission from REF.[26], APS; panel **b** reprinted with permission from REF.[42], Wiley; panel **c** reprinted with permission from REF.[49], APS.

and of a superconducting layer has been demonstrated[37]. This has inspired the realization of bilayer thermal cloaks in three[38] and two dimensions[39] (FIG. 1b). A bilayer thermal cloak consists of an inner layer ($R_1 < r < R_2$) and an outer layer ($R_2 < r < R_3$) with conductivities κ_2 and κ_3, respectively. The inner layer is assumed to be a perfect thermal insulator ($\kappa_2 \to 0$), which ensures that the external heat flux does not penetrate inside it. The outer layer must then eliminate the distortion of the external field. Directly solving the thermal conduction equation gives $\kappa_3 = \kappa_0(R_3^3 + 0.5R_2^3)/(R_3^3 - R_2^3)$ for a spherical cloak and $\kappa_3 = \kappa_0(R_3^2 + R_2^2)/(R_3^2 - R_2^2)$ for a cylindrical cloak. If any two parameters out of κ_3, κ_0 and R_3/R_2 are known, the third parameter can be uniquely determined. A different type of bilayer cylindrical device was recently proposed[22], with an extremely conductive inner layer with $\kappa_2 \to \infty$, such that heat is quickly transported through it, irrespective of the object inside. This mechanism is reminiscent of the tunnelling effect of near-zero-index materials in photonics, and a rigorous correspondence has indeed been proven between the two[22]. The outer layer also in this case compensates for the distortion to the external field, with $\kappa_3 = \kappa_0(R_3^2 - R_2^2)/(R_3^2 + R_2^2)$. An object inside this thermal cloak has good sensitivity to environmental changes.

Inspired by these bilayer cloaks, a multiphysics cloak[40] and a multiphysics invisible sensor[41], which can manipulate heat flux and electric current simultaneously, have been realized. By modifying the bilayer structure, thermal camouflaging has been demonstrated to create multiple images of an object in heat conduction away from its actual position[42]. Based on scattering theory, thermal transparency[43] and passive metashells with adaptive thermal conductivities[44] have also been proposed. By directly solving the conduction equation in the elliptical coordinate system (ξ,η), the bilayer strategy has been successfully applied to the design of an elliptical cloak, with the assumption of an anisotropic background[45]. Instead of analytically solving the governing equations, optimization algorithms can be used to obtain the structure that gives a certain temperature distribution, as demonstrated in the design of a topology-optimized thermal carpet cloak[46]. When different materials are combined to realize bilayer or multilayer thermal devices, the interfacial thermal resistance may influence their performance[47].

Temperature dependence. The thermal conductivities of most materials depend on temperature. For some phase-change materials, this temperature dependence is marked and can be used to build thermal diodes, regulators and switches[48]. Traditional transformation theories[8,9,25] only apply to linear materials whose thermal conductivity is independent of temperature. This issue was resolved by proving that the temperature-dependent Fourier's law still maintains form invariance under coordinate transformation[49,50]. Therefore, the nonlinear thermal conductivity in real space is obtained as $\kappa(T) = A\kappa'(T)A^{\mathrm{T}}/\det(A)$, which has the same form as for temperature-independent cases[8,9,25]. Furthermore, it was proposed that the equation can be equivalently written as $\kappa(T) = A(T)\kappa_0 A(T)^{\mathrm{T}}/\det[A(T)]$, where $A(T)$ corresponds to a temperature-dependent transformation[49]. This equation can be used to design devices such as switchable thermal cloaks[49] and concentrators[51]. A macroscopic thermal diode was designed and fabricated using parts of a switchable thermal cloak[49] (FIG. 1c). In addition, a temperature-dependent transformation was used to design multifunctional devices, such as a thermal cloak–concentrator[52]. Without relying on transformation, an energy-free thermostat was designed by studying the temperature-dependent one-dimensional (1D) thermal conduction[53], in which a temperature-trapping effect was found to maintain near-constant temperature for various boundary conditions. This device can be used for the temperature management of targets subject to large temperature differences.

Strong temperature-dependent thermal conductivity is not easily found in natural materials. Therefore, the experimental demonstration of the devices above relied on the large mechanical deformation afforded by shape-memory alloys across a phase transition, which effectively modifies the thermal conductivity by changing the contact area between components. Shape-memory alloys are widely used to make thermal switches and diodes[48], thanks to their near-room-temperature and tunable phase transition point, and to their configurable deformation patterns. One interesting application is thermal management exploiting thermal regulators based on shape-memory alloys to increase the safety and capacity of Li-ion batteries[54]. Phase-change nanocomposites are also promising materials. Based on one such material, a temperature-responsive thermal metamaterial with a modular design has been demonstrated to manage the temperature field on a circuit board with switchable heat-shielding effects[55].

Between the macroscale and the microscale. Conductive thermal metamaterials are different from other kinds of metamaterials in many ways. First, they manipulate diffusion instead of wave propagation. Second, they contain no sub-wavelength structures. Finally, because there is no such mechanism as local resonances, the effective material parameters (thermal conductivity, mass density, heat capacity) are not easily adjustable, let alone unconventional (negative or zero). The lack of some features typical of metamaterials simplifies design and fabrication, but also restricts performance and applications. A major challenge is to break these restrictions and discover new mechanisms for the control of macroscopic heat conduction.

Some opportunities may exist at the microscale. For example, the thermal conductivity of silicon nanowires can be locally tuned to any desired value between 2 and 50 $\mathrm{W\,m^{-1}\,K^{-1}}$ with a suitable dose of helium ion irradiation[56], which introduces point defects and triggers a crystalline–amorphous transition beyond a threshold. Moreover, the defects can be annealed at high temperatures, making the engineering process reversible to some extent. A continuously addressable thermal conductivity profile can thus be built in a single material while maintaining a uniform morphology. This process is more feasible than the design of discrete and fixed distribution of materials properties common in most conductive thermal metamaterials. As a demonstration, bilayer and trilayer thermal cloaks have been fabricated on a $20 \times 20\,\mu\mathrm{m}$ silicon membrane by using the ion irradiation mechanism[57] (Fourier's law is still valid at this length scale).

More microscopic mechanisms for thermal conductivity engineering are discussed in the next section. Also, active sources such as electric fields, pressure and chemical stimulation enable reversible and even dynamic tuning of the thermal conductivity (see the section on the active manipulation of heat transfer). However, little effort has been made so far to engineer thermal conductivity with spatial variations.

Microscopic approaches

Phonons — quasiparticles representing the collective vibrational modes of materials — are one of the main heat carriers in semiconductors and dielectric materials. The emerging field of nanophononics aims to manipulate thermal properties by controlling phonon behaviours. Based on the phonon Boltzmann transport equation, the thermal conductivity under the single-mode relaxation time approximation can be expressed as

$$\kappa = \frac{1}{24\pi^3} \sum_n \int C(\mathbf{k}, n, T) v_{\mathrm{g}}^2(\mathbf{k}, n) \tau(\mathbf{k}, n, T) \mathrm{d}\mathbf{k} \qquad (4)$$

where n is the dispersion branch index, $\mathbf{k}$ is the phonon wave vector, T is the temperature, C is the phonon specific heat of each mode, v_{g} is the group velocity and τ is the phonon lifetime. The group velocity v_{g} is defined as the derivative of the phonon dispersion: $v_{\mathrm{g}} = \partial\omega/\partial k$. The summation over the dispersion branch index n can also be replaced by an integral over the frequency ω multiplied by the density of states.

A widely used approach to manipulate heat conduction is to modify phonon lifetime, which can be done, for example, by doping or by changing the surface roughness. Another potential approach is to modify the phonon properties by designing nanostructured devices, which is challenging owing to the short wavelength of the dominant thermal phonons, but has attracted intense interest amid the recent progress in nanofabrication. The wave nature of phonons is exploited in two types of systems that are the object of substantial current interest: nanophononic crystals and nanophononic metamaterials.

Nanophononic crystals. Phononic crystals are artificial periodic nanostructures whose periodicity is on the order of the phonon wavelength[58]. To distinguish phononic crystals that manipulate thermal phonons from those that influence elastic waves, the former are usually referred to as nanophononic crystals (NPCs). NPCs can be 1D (superlattices, in which the periodical change in material properties only happens in one direction, FIG. 2a), 2D (nanomeshes, FIG. 2b) or 3D (FIG. 2c). The wave interference induced by these periodic structures can give rise to many phenomena that are not observed in conventional bulk materials, such as Brillouin zone folding and bandgap opening. There are three important length scales in NPCs with smooth boundaries (FIG. 2b): the phonon wavelength (λ), the phonon mean free path (MFP, Λ) and the periodicity of the phononic crystal (d). Depending on the relative magnitude of these quantities, phonon transport can be categorized into three regimes: if the periodicity is smaller than the phonon wavelength ($d < \lambda$), wavelike phonon interference induced by coherent scattering (Bragg diffraction) is dominant; if the periodicity is larger than the phonon MFP ($d > \Lambda$), particle-like diffusive scattering is dominant; if the periodicity is larger than the phonon wavelength but smaller than its MFP ($\lambda < d < \Lambda$), the relative contribution of phonon interference and diffusive scattering to heat transport is a matter of debate. It is also worth pointing out that in this last regime some phonons undergo particle-like ballistic transport, which has motivated the development of ray-like heat manipulation in phononic nanostructures, such as in directional phonon sources and thermal lenses[59–61].

For 1D NPCs, it was observed that the thermal conductivity of a W/Al_2O_3 superlattice is up to four times smaller than the series average of the conductivities of the alumina and tungsten layers[62]. The crossover from diffusive to coherent phonon scattering, marked by a

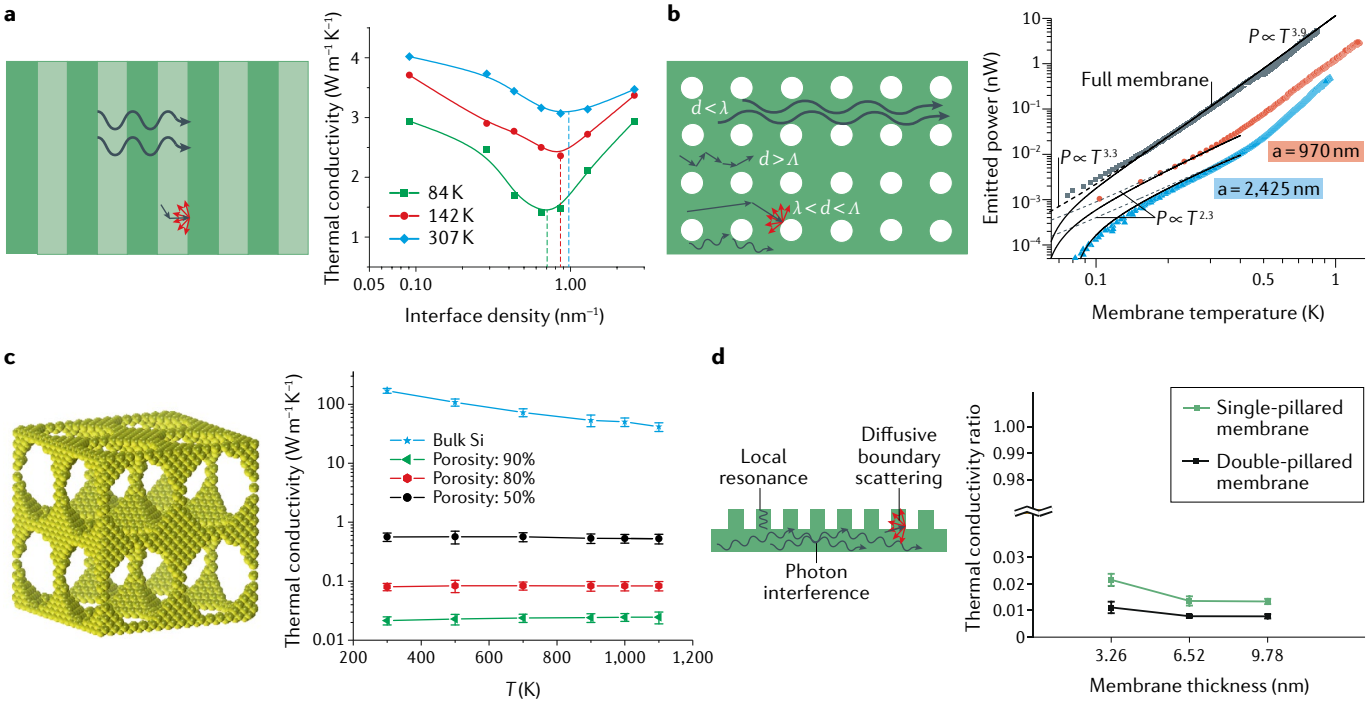

Fig. 2 | **Microscopic approaches to heat conduction. a** | Coherent (wavy lines) and diffusive (straight lines) phonon scattering in 1D superlattices (left). Measured thermal conductivity in $(SrTiO_3)_m/(CaTiO_3)_n$ superlattices as a function of the density of interfaces at different temperatures. The minimum thermal conductivity marks the crossover from diffusive to coherent phonon scattering. The minimum thermal conductivity is lower at lower temperatures, and the corresponding density of interfaces is also smaller, consistent with the observation of coherent wave effects[65] (right). **b** | The three possible regimes of phonon transport in a 2D nanophononic crystal (NPC), which are determined by the relationship between phonon wavelength λ, phonon mean free path Λ and periodicity d of the NPC (left). Measured emitted phonon power P as a function of temperature. The grey squares indicate data for the full membrane, the red circles and blue triangles data for two square NPC samples with periodicity a of 970 nm and 2,425 nm, respectively. Theoretical calculations with and without phonon back radiation power from the substrate are represented by the solid and dashed lines, respectively. At low temperature, the temperature dependence of the conductance is different for the full membrane ($P \propto T^{3.3}$) and for the NPCs ($P \propto T^{2.3}$)[69] (right). **c** | A 3D NPC (left). Thermal conductivity of 3D NPCs with various porosities and of bulk Si as a function of temperature. When the porosity of the NPC is 90%, the thermal conductivity as predicted from the classical Eucken model is about 12 W m^{-1} K^{-1}, three orders of magnitude larger than that calculated by equilibrium molecular dynamics, which is in turn almost four orders of magnitude lower than that of bulk Si (REF.[77]). The error bar is the standard deviation of 12 simulations with different initial conditions (right). **d** | Schematic illustrating the three mechanisms that induce a reduction in the thermal conductivity of pillar-based structures (left). A double-pillared membrane (with pillars on both sides) and a single-pillared membrane (with pillars on one side only) have a thermal conductivity two orders of magnitude lower than a uniform membrane with the same thickness[84]. The thermal conductivity predictions are the average of six simulations with different initial conditions in the two orthogonal directions of the membrane. The error bar is the standard deviation of the 12 predicted values (right). Panel **a** adapted from REF.[65], Springer Nature; panel **b** adapted from REF.[69], Springer Nature; panel **c** adapted with permission from REF.[77], ACS; panel **d** adapted from REF.[84], Springer Nature.

minimum in the thermal conductivity as a function of period thickness, was predicted[63,64] and then observed in epitaxial oxide superlattices[65] (FIG. 2a). For 2D NPCs, a large reduction in thermal conductivity compared with bulk materials was observed in a wide temperature range, between 0.1 K and 300 K (REFS[13,66–75]). For 3D NPCs, an extremely low thermal conductivity was predicted for silicon crystals with spherical pores, even at temperatures up to 1,100 K (REFS[76–78]) (FIG. 2c). The remarkable reduction of thermal conductivity in 2D and 3D NPCs cannot be simply explained by taking porosity into account[66,77]. 2D NPCs, in particular, are being actively investigated in experiments.

At low temperature, phonon interference causes the strong difference in the temperature dependence of the thermal conductance of a full membrane and of 2D NPCs[69] (FIG. 2b). At room temperature, the role of phonon interference is still debated. Both phonon interference and diffusive scattering can induce a decrease of the thermal conductivity. For phonon interference, the reduction originates from the decrease of the group velocity v_g as a consequence of the flattening of the phonon band structure[13,67–69,79]. For diffusive scattering, the reduction is due to the decrease of phonon MFP and lifetime[66–68,73,74,79]. In experiments, methods to distinguish between these two mechanisms include studying the thermal conductivity of NPCs with fixed periodicity but different unit cell geometries[70,72] or of periodic and aperiodic nanomeshes with the same porosity[74,75]. No unambiguous conclusion has been yet reached, because both a partially coherent scattering model[70,79] and a diffusive scattering model[74,80,81] show good agreement with experimental results.

The inconsistency arises from an insufficient knowledge of the coherent length. Detecting phonon interference by measuring thermal conductivity is an indirect method. Owing to the short wavelength of thermal phonons, a small difference in the geometry or surface roughness of NPCs can greatly modify the phonon coherence length, which may lead to contradictory conclusions in different experiments. A direct detection of phonon coherence would provide more information. Recently, the use of two-photon interference methods such as coherent population trapping and electromagnetically induced transparency has been proposed to measure the phonon coherence length[82].

Nanophononic metamaterials. Nanophononic metamaterials (NPMs) use local resonances to manipulate heat conduction. The reduction of thermal conductivity in NPMs was first revealed in pillar-based structures[14]. A study of the optimal size and geometry of NPMs showed a reduction of the thermal conductivity of up to two orders of magnitude compared with non-nanostructured membranes[83,84] (FIG. 2d). The concept of NPM has also been applied to nanoribbons[85] and nanotubes[86]. External periodic pillars acting as local resonators are deposited on a base material, introducing additional flat branches with their own resonance frequencies to the phonon dispersion of the base material. The hybridization between the local resonances of the pillars and the vibrational modes of the base material induces avoided crossings in the phonon dispersion, opening bandgaps and flattening the original branches near the resonance frequencies, and hence lowering the group velocity and thermal conductivity. NPMs have some potential advantages over NPCs for the design of thermoelectric devices. The externally deposited pillars have a small effect on the electron transport of the base material and do not decrease the device's mechanical strength. Moreover, a membrane with periodic pillars can be treated as an NPC with an extra degree of freedom. For the detailed analysis of geometry and size effects in NPMs and a direct comparison between NPMs and NPCs, we refer the interested reader to a recent comprehensive review[87].

Although the reduction of the thermal conductivity has been observed in both experiments[88] and numerical simulations[14,83,89–93], the role of local resonances is still debated. Three mechanisms are conjectured as possibly underlying the reduced thermal conductivity: local resonances; phonon interference induced by coherent scattering; and diffusive boundary scattering (FIG. 2d).

To remove the effect of phonon interference, researchers numerically studied the thermal conductivity of membranes with aperiodic pillars[90]. The observed very low thermal conductivity indicates that the contribution of phonon interference is small, but cannot distinguish between the contribution of local resonances and of diffusive boundary scattering. Distinguishing between these two contributions requires fabricating pillars with no local resonances in the frequency region of the dominant phonons, a type of sample that has rarely been studied experimentally. Another approach to uncover the relative contribution of the three mechanisms is to study the dependence of the thermal conductivity on the pillar height[83,89,92,93]. Molecular dynamics (MD) simulations showed that periodic pillars as short as a few angstroms can cause a drop of more than 50% in thermal conductivity[89,93]. In such short pillars, almost no local resonance frequencies are inside the frequency region of the dominant phonons. This fact suggests that the existence of periodicity (phonon interference) contributes to the reduced thermal conductivity. As the pillar height increases, the results of MD simulations and of finite element method (FEM) simulations become inconsistent. Whereas MD simulations indicate that the reduction gradually saturates[89,93], FEM shows that the thermal conductivity increases after a critical pillar height[92]. This inconsistency, which may be due to the lack of anharmonic phonon–phonon interactions in FEM simulations, points to a possible role of diffusive scattering.

The mechanism behind the reduced thermal conductivity of pillar-based NPMs thus remains an open question. It is hard to isolate the contribution of local resonances, phonon interference and diffusive scattering in experiments. As in the case of NPCs, a direct detection of the phonon coherence length can provide more useful information.

Finally, another kind of resonance, due to the coupling of longitudinal and transverse modes, was used to reduce the thermal conductivity in core–shell nanowires[94].

Manipulating thermal radiation

Thermal radiation is ubiquitous, and is at the base of a fundamental heat transfer mechanism[95–97]. Any object at finite temperature emits thermal radiation due to the thermally induced motion of particles and quasi-particles. Conventional thermal emitters have a set of common characteristics[97] (FIG. 3a) and fundamental constraints (BOX 2) that restrict their capability to control heat transfer processes.

Recent advances in using sub-wavelength structures have led to properties that are very different from those of conventional materials. Moreover, in the near-field regime, in which the gap size is comparable or smaller than the thermal wavelength, radiative heat transfer can be significantly larger than in the far field. These approaches provide new capabilities for controlling fundamental aspects of thermal radiation, and open up new opportunities for applications. In this section, we give a

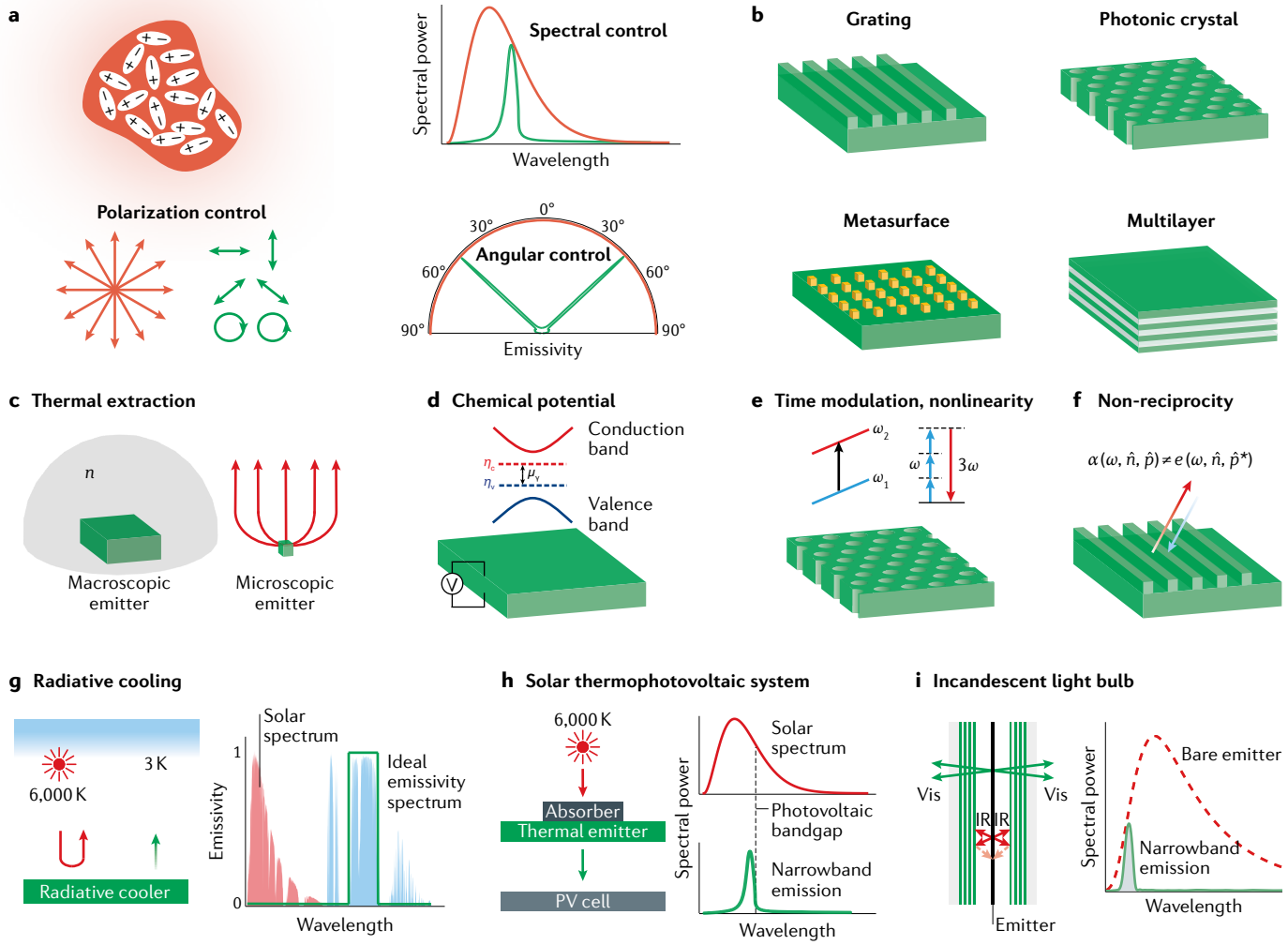

Fig. 3 | **Far-field thermal radiation manipulation. a** | Conventional blackbody thermal radiation (orange) and nanostructure-controlled thermal radiation (green). Conventional blackbody thermal radiation typically has broadband, broad angle and unpolarized characteristics. By contrast, nanostructure-controlled thermal radiation can be narrowband, have a narrow angle range and be polarized. **b** | Nanostructures for thermal radiation control, including photonic crystals, gratings, metamaterials and multilayer films. **c** | Beyond Planck's Law: enhancing the absorption cross-section with thermal extraction in macroscopic emitters and microscopic thermal antennas. A transparent hemispherical dome with refractive index n can be used to enhance the absorption cross-section of a macroscopic emitter by a factor n^2 (left). A microscopic thermal antenna can have an absorption cross-section significantly larger than its geometrical cross-section (right). **d** | Non-equilibrium thermal radiation can be obtained in a semiconductor with a non-zero chemical potential μ_γ, determined by the separation of the quasi-Fermi levels for electrons, η_c, and holes, η_v. **e** | Non-equilibrium thermal radiation can be realized using time-modulation-induced frequency transitions and nonlinearities (for example, a transition from ω_1 to ω_2 under time modulation, and from ω to 3ω under third-order nonlinearity). **f** | Beyond Kirchhoff's law: non-reciprocal thermal radiation. The balance between angular spectral absorptivity $\alpha(\omega, \hat{n}, \hat{p})$ and emissivity $\varepsilon(\omega, \hat{n}, \hat{p}^*)$ can be broken in non-reciprocal systems. **g** | Daytime radiative cooling can be achieved using materials with a near-zero absorptivity over the entire solar spectrum and a strong emissivity in the 8–13 μm spectral range. **h** | A solar thermophotovoltaic system: an intermediate element absorbs the incoming sunlight to heat up, and then generates thermal emission tailored to the solar-cell bandgap. **i** | In an incandescent light bulb, the efficiency can be significantly improved by suppressing the near-infrared (IR) emission while allowing the visible light (vis) emission. Panel **i** adapted from REF.[132], Springer Nature.

Box 2 | **Fundamental properties of thermal radiation**

Planck's law

The thermal emission power P_0 of a blackbody emitter in thermal equilibrium at temperature T, emitting into free space, is described by Planck's law:

$$P_0 = A \cdot \frac{\omega^2}{4\pi^2 c^2} \cdot \frac{\hbar\omega}{e^{\hbar\omega/k_B T} - 1} \quad (5)$$

where A is the area of the emitter, ω is the angular frequency of the emission, $\hbar$ is the reduced Planck constant, k_B is the Boltzmann constant and c is the speed of light in vacuum.

Absorptivity and emissivity

The key quantities characterizing thermal emitters in the far field are the angular spectral absorptivity $\alpha(\omega, \hat{\mathbf{n}}, \hat{\mathbf{p}})$, and the angular spectral emissivity $\varepsilon(\omega, \hat{\mathbf{n}}, \hat{\mathbf{p}})$. $\alpha(\omega, \hat{\mathbf{n}}, \hat{\mathbf{p}})$ represents the absorptivity of the emitter for incident light at a frequency ω, with a direction $\hat{\mathbf{n}}$ and with a polarization vector $\hat{\mathbf{p}}$, and is measured as the ratio between the incident and the absorbed power per unit area. $\varepsilon(\omega, \hat{\mathbf{n}}, \hat{\mathbf{p}})$ measures the spectral emission power per unit area at a certain ω, $\hat{\mathbf{n}}$ and $\hat{\mathbf{p}}$, normalized against the spectral emission power per unit area of a blackbody emitter at the same ω, $\hat{\mathbf{n}}$, and $\hat{\mathbf{p}}$. Thus for a blackbody, both $\alpha(\omega, \hat{\mathbf{n}}, \hat{\mathbf{p}})$ and $\varepsilon(\omega, \hat{\mathbf{n}}, \hat{\mathbf{p}})$ are equal to 1. For typical macroscopic thermal emitters, $\alpha(\omega, \hat{\mathbf{n}}, \hat{\mathbf{p}})$ and $\varepsilon(\omega, \hat{\mathbf{n}}, \hat{\mathbf{p}})$ are between 0 and 1.

Kirchhoff's law

The angular spectral absorptivity and emissivity typically satisfy Kirchhoff's law:

$$\alpha(\omega, \hat{\mathbf{n}}, \hat{\mathbf{p}}) = \varepsilon(\omega, \hat{\mathbf{n}}, \hat{\mathbf{p}}^*) \quad (6)$$

where the asterisk in $\hat{\mathbf{p}}^*$ denotes complex conjugation. Equation 6 is valid for reciprocal systems consisting of materials characterized by symmetric permittivity and permeability tensors.

Far-field and near-field radiative heat transfer

Taking the simple example of two semi-infinite parallel plates separated by a vacuum gap of size d, the radiative heat flux density q, or the radiative heat flux across the gap per unit area is[294]

$$q = \int_0^\infty \frac{d\omega}{4\pi^2}[\Theta(\omega, T_1) - \Theta(\omega, T_2)] \int_0^\infty dk[\xi_s(\omega, k) + \xi_p(\omega, k)]k \quad (7)$$

where $\Theta(\omega, T) = \hbar\omega/[\exp(\hbar\omega/k_B T) - 1]$ and k is the wave vector parallel to the planar surfaces. $\xi_s(\omega, k)$ and $\xi_p(\omega, k)$ are the photon transmission probabilities for the transverse electric (s) and transverse magnetic (p) polarizations, respectively, and can be written as:

$$\xi_{s,p}(\omega, k < k_0) = \frac{(1 - |r_1|^2)(1 - |r_2|^2)}{|1 - r_1 r_2 e^{-2ik_{z0}d}|^2} \quad (8)$$

for propagating waves, and

$$\xi_{s,p}(\omega, k > k_0) = \frac{4\mathrm{Im}(r_1)\mathrm{Im}(r_2)e^{-2|k_{z0}|d}}{|1 - r_1 r_2 e^{-2ik_{z0}d}|^2} \quad (9)$$

for evanescent waves. In equations 8 and 9, $k_0 = \omega/c$ is the free-space wavenumber and k_{z0} is the out-of-plane wavenumber in vacuum. The parameters $r_{1,2}$ are the Fresnel reflection coefficients for incidence from the gap to bodies 1 and 2. Both ξ_s and ξ_p are between 0 and 1. In most radiative heat transfer cases with non-magnetic materials, $\xi_p(\omega, k)$ dominates. As a result, the summed photon transmission probability $\xi(\omega, k) = \xi_s(\omega, k) + \xi_p(\omega, k)$ is typically between 0 and 1.

In the far-field regime, only propagating waves (equation 8) contribute to the total heat flux. In the near-field regime, when the gap size is smaller than the characteristic thermal wavelength, evanescent waves (equation 9) also contribute (FIG. 4a). As a result, the flux density in the near-field regime can exceed that in the far-field regime by orders of magnitude.

brief overview of some fundamental advances in manipulating both far-field and near-field thermal radiation, and highlight some applications.

Far-field thermal radiation control

Fundamental properties control. In nanostructures in which the feature sizes are comparable to the thermal radiation wavelength (FIG. 3b), one can design the structure to control all aspects of the emissivity $\varepsilon(\omega, \hat{\mathbf{n}}, \hat{\mathbf{p}})$ (REFS[15,98–105]). For example, to control the spectral characteristics, one can strongly suppress thermal emissivity at a certain frequency using a photonic bandgap[98,99]. One can also strongly enhance the emissivity of a material using a variety of photonic resonators[100,103]. A lossy resonator can create a spectrally sharp absorption peak and therefore a narrowband thermal emission peak. Moreover, by constructing multiple resonances, strong thermal emission with multiband or broadband characteristics can be achieved[101,103,105]. As an example of control of the angle and polarization characteristics, strongly angular-dependent thermal radiation has been demonstrated in a SiC grating[15]. One can also achieve strongly polarized thermal radiation by constructing polarization-dependent resonances. Thermal emission with linear, circular and arbitrary polarization can be obtained with anisotropic, chiral and spin-optical metasurfaces[102].

Planck's law (equation 5 in BOX 2) sets an important constraint for the power of far-field thermal radiation. A photonic structure can have very different absorption and geometric cross-sections. Super-Planckian radiation can be realized when the absorption cross-section exceeds the geometric cross-section, as has been demonstrated in microscopic thermal antennas[106–108] and in macroscopic emitters using a thermal extraction scheme[109] (FIG. 3c). Efforts have also been made to extract near-field thermal radiation into the far field[109–111].

Non-equilibrium thermal emitters offer the possibility of controlling radiation beyond equilibrium systems. One example of a non-equilibrium thermal emitter is an electrically biased or optically excited semiconductor, within which the electrons and holes can have different quasi-Fermi levels, resulting in a non-zero chemical potential μ_γ (FIG. 3d). Such a semiconductor emits with a spectral energy density $\rho(\omega)$ (REF.[112]):

$$\rho(\omega) = \frac{\omega^2}{\pi^2 c^3} \frac{\hbar\omega}{e^{(\hbar\omega - \mu_\gamma)/k_B T} - 1} \quad (10)$$

The Planck's distribution is recovered at $\mu_\gamma = 0$. At the same emitter temperature, a positive chemical potential leads to a $\rho(\omega)$ significantly beyond the one predicted by the Planck's distribution. By contrast, a negative chemical potential leads to a significantly suppressed $\rho(\omega)$. The manipulation of the photon chemical potential offers new opportunities in heat manipulation using optoelectronic technology, as we discuss further in the near-field thermal radiation section.

Non-equilibrium thermal emission also occurs in a temporally modulated thermal emitter[113] if the modulation timescale is significantly smaller than the thermal time constant. Using such an emitter, heat can be actively pumped from a cold emitter to a hot emitter, resulting in a photon-based active cooling mechanism. A closely related approach to realize non-equilibrium thermal emitters is to exploit nonlinear effects[114,115] (FIG. 3e).

The vast majority of thermal emitters satisfy Kirchhoff's law (equation 6 in BOX 2), because most materials are reciprocal. This imposes significant constraints in solar energy harvesting: an efficient absorber

is also an efficient emitter, and therefore must re-emit part of the energy, which represents an intrinsic loss mechanism. The thermodynamic limit of solar energy harvesting can only be reached by breaking Kirchhoff's law[116,117]. Near-complete violation of Kirchhoff's law can be achieved by combining resonant nanostructures with magneto-optical materials[118] (FIG. 3f). Nonlinear or time-varying permittivity and permeability can be used to break the balance between absorptivity and emissivity.

Applications. The advances in far-field thermal radiation manipulation have led to many important applications[5]. In this section, we highlight three examples: daytime radiative cooling, thermophotovoltaic systems and incandescent lighting.

The Universe, at 3 K, represents the ultimate heat sink. Thermal radiation enables access to the cold Universe: the blackbody radiation at typical ambient temperature has a large spectral overlap with the transparency window of the Earth's atmosphere in the wavelength range of 8–13 μm. Thus, any object on Earth, given sky access, can radiate heat out to the Universe, resulting in radiative cooling. Although night-time radiative cooling has been known for centuries, daytime radiative cooling is more desirable and also more challenging owing to the fact that the Sun heats up most materials during the day. Achieving daytime radiative cooling requires a near-zero absorptivity over the entire solar spectrum and a strong emissivity in the 8–13 μm region (FIG. 3g). A daytime radiative cooler with this spectral features has been theoretically proposed[119] and experimentally demonstrated[120]. Since then, there has been considerable progress towards large-scale deployment of this technology[121–124]. With its ability to harness the coldness of the Universe and its broad implications for energy technology[125], radiative cooling has now opened up a new frontier in renewable energy research[126].

In the area of solar energy harvesting, single-junction solar cells are subject to an efficiency limit of 41%, known as the Shockley–Queisser limit. An important energy loss arises from the mismatch between the broadband solar radiation and the intrinsic properties of single-junction solar cells. Solar thermophotovoltaic (STPV) systems represent an important avenue towards overcoming the Shockley–Queisser limit[127]. In a STPV system, an intermediate element absorbs the incoming sunlight, heats up, and then generates thermal emission tailored to the solar cell bandgap (FIG. 3h), increasing the theoretical efficiency limit to 85%[128]. Proof-of-principle demonstrations of such a concept have been reported[129,130]. Closely related to STPV systems, thermophotovoltaic (TPV) systems can use thermal radiation from a local heat source to generate electricity in a photovoltaic cell[131]. In TPV systems, instead of suppressing below-bandgap radiation, one can perform below-bandgap photo recycling, using a photovoltaic cell with minimum below-bandgap absorption and a high-quality back reflector[131]. Further improvements in the photonic, thermal and carrier management of emitters and cells and in the manufacturing and integration of high-quality materials may ultimately push STPV and TPV systems towards practical implementation.

In the area of incandescent lighting systems, conventional incandescent light bulbs have low efficiency, because the thermal radiation they emit is mostly in the infrared wavelength range, and only a small portion produces visible light that can be used for lighting purposes. One way to reduce this loss is to suppress the near-infrared emission while allowing the visible light emission (FIG. 3i). An experimental demonstration of this concept[132] showed an efficiency approaching that of commercial fluorescent or light-emitting diode bulbs. The performance can be further improved with spectral engineering and optimization[133,134].

Near-field radiative heat transfer control

Heat transfer in the near field (FIG. 4a) can exceed the far-field blackbody limit by orders of magnitude[135–139] (BOX 2). In this section, we briefly review the recent advances and application opportunities in near-field thermal radiation.

Enhancing near-field radiative heat transfer. Based on equation 7 in BOX 2, to enhance the overall heat transfer, one needs to maximize the photon transmission probability $\xi(\omega, k)$ over all accessible frequency ω and parallel wave vector k channels. The theoretical maximum heat transfer can be intuitively understood by looking at an ω–k diagram (FIG. 4b). For two planar bodies with gap distance d, the maximum accessible parallel wave vector k for photon transmission is $\sim 1/d$ (REF.[140]). This defines a region in the ω–k space within which the photon transmission channels are accessible. Such a treatment provides an intuitive understanding of the $1/d^2$ scaling of the magnitude of the heat transfer coefficient in the near-field regime, as well as an optimistic upper bound for the heat transfer coefficient[140].

To physically realize such a large enhancement in near-field radiative heat transfer (NFRHT), one can choose materials that support surface waves such as surface phonon polaritons (SPhPs) and surface plasmon polaritons (SPPs) to access the large-k channels. For example, one can use polar dielectrics such as SiC and SiO_2 that support SPhPs[141], or doped semiconductors such as Si that support SPPs[142]. A plot of the photon transmission probability $\xi(\omega, k)$ between a pair of SiC slabs with a gap distance of 10 nm is shown in the left panel of FIG. 4c. Owing to the surface wave excitation, a substantial number of $\xi(\omega, k)$ channels can be accessed in the regime in which k is orders of magnitude larger than k_0. By contrast, such a typical surface mode only uses a small fraction of the ω–k space, which limits the overall heat transfer enhancement.

To enhance NFRHT, nanostructures and more complex geometries have been explored (FIG. 4d–h). The first approach is to carefully engineer the surface wave mode so that it has the desired frequency and loss. The maximum heat flow can be achieved[143] with spectrally matched emitters and receivers when the dielectric function ε on both sides approaches $-1 + i\alpha$, where $\alpha \ll 1$. An important consideration is that ideally one should choose the excitation energy of the surface wave mode to be close to $k_B T$, where the thermal photon population is largest. As a result, Si-based metasurfaces (FIG. 4d)

featuring 2D periodic arrays of holes can exhibit a room-temperature NFRHT coefficient much larger than that of any unstructured material[144]. Introducing holes in the Si layers reduces the losses and the effective plasma frequency, which, in turn, redshifts the surface modes. This way, the surface modes are more easily occupied at room temperature, leading to NFRHT enhancement.

Another approach is to increase the number of resonant modes using multi-resonance nanostructures. The right panel of FIG. 4c shows how multiple modes can be constructed to fill a larger portion of the ω–k space. Metasurfaces, photonic crystals[145], grooves[146] (FIG. 4f) and multilayer[147] structures (FIG. 4g) can all be designed for this purpose. For example, NFRHT between multilayer thermal bodies (FIG. 4g) can be enhanced by surface states at multiple surfaces[147]. There are also efforts to use hyperbolic dispersion to broaden the filling of the ω–k space to enhance NFRHT[148].

Despite all the efforts so far, there are two important open questions in our understanding of NFRHT. First, from the fundamental point of view, the NFRHT upper bound that we have discussed (FIG. 4b) is apparently a very optimistic limit[140]. Is there a tighter bound to accurately describe the fundamental limit of NFRHT?

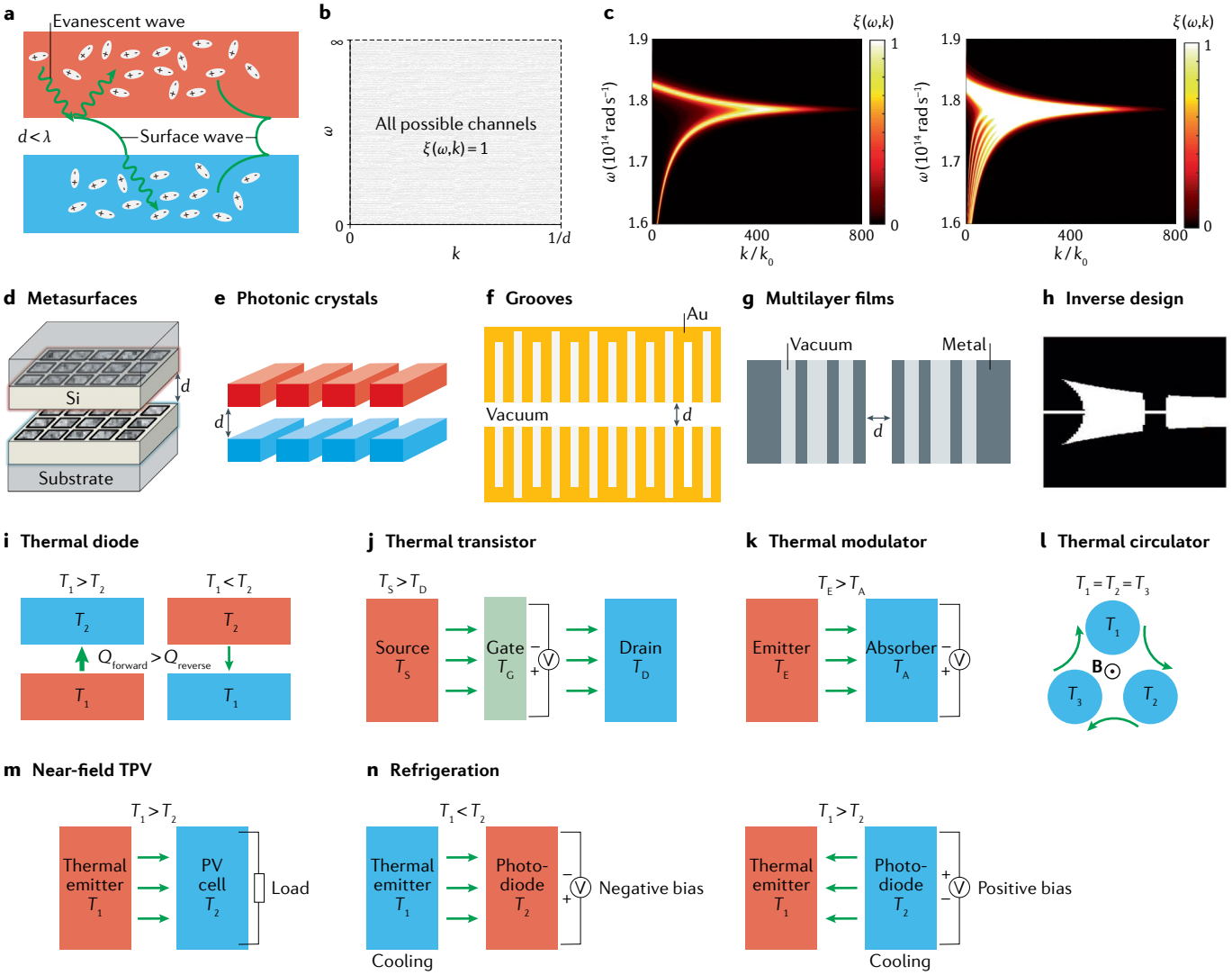

Fig. 4 | **Near-field thermal radiation manipulation. a** | Schematic of near-field radiative heat transfer across a vacuum gap of size d comparable to or smaller than the peak thermal wavelength λ. Evanescent waves and surface waves provide additional heat-transfer channels and significantly enhance heat transfer. **b** | Theoretical limit of near-field heat transfer with all possible channels over the frequency–wave vector (ω–k) space. **c** | A plot of photon transmission probability $\xi(\omega, k)$ between a pair of SiC slabs separated by a gap of 10 nm. A standard surface mode enhances the heat transfer in the large-k regime but only uses a small fraction of the ω–k space (left). Near-field heat transfer enhancement based on multiple modes constructed from a multilayer structure to fill a larger region of the ω–k space. k_0 is the free-space wavenumber (right). **d**–**h** | Platforms for enhancement of near-field heat transfer include metasurfaces (panel **d**), photonic crystals (panel **e**), grooves (panel **f**), multilayer films (panel **g**) and structures obtained with inverse design (panel **h**). **i**–**n** | Concepts for near-field heat transfer devices include the thermal diode (panel **i**), thermal transistor (panel **j**), thermal modulator (panel **k**), thermal circulator (panel **l**), near-field thermophotovoltaic (TPV) devices (panel **m**), and near-field negative and positive luminescent refrigerators (panel **n**). **B**, magnetic field; PV, photovoltaic; Q, heat; T, temperature. Panel **d** adapted with permission from REF.[144], APS; panel **e** reprinted with permission from REF.[145], APS; panel **f** reprinted with permission from REF.[146], APS; panel **g** adapted with permission from REF.[147], APS; panel **h** reprinted with permission from REF.[152], APS.

There have been some recent efforts to address this question[149–151]. Second, from the structure design point of view, can we design structures that use the ω–k space more effectively and move beyond the existing designs? A promising direction is based on the inverse design of complex nanostructures[152] (FIG. 4h).

Near-field heat transfer manipulation. NFRHT has become a promising approach for manipulating heat transfer at the nanoscale. In analogy with the key components in electronic circuits, here we review key components for near-field heat manipulation, including thermal diodes, transistors, modulators and circulators, along with potential applications in nanoscale thermal management and energy harvesting.

A thermal diode is a two-terminal device in which the magnitude of the thermal conductance depends on the direction of the heat flow (FIG. 4i). To realize an NFRHT thermal diode, the key is to use materials or structures with electromagnetic properties with different temperature dependence at the two terminals. For example, the different temperature dependence of the dielectric functions of two SiC polytypes can lead to either alignment or misalignments of SPhP resonances across the vacuum as one changes the direction of the thermal bias, resulting in NFRHT rectification[153]. Phase-change materials can also be used for this purpose[154–156].

In a thermal transistor (FIG. 4j), a temperature bias on the gate is used to modulate the heat flux between the source and the drain. Implementing a gate with a phase-change material, thermal switching, modulating and amplifying can be achieved[157]. In addition to the thermal transistor, heat transfer can be directly modulated with a two-terminal thermal modulator (FIG. 4k) by controlling the material or resonant properties of at least one terminal. To realize a NFRHT modulator, a lot of concepts used in the dynamic control of far-field thermal radiation can be directly applied, including the use of phase-change materials and field effects (discussed in the section on the active manipulation of heat transfer).

Breaking reciprocity can have important consequences in NFRHT: for example, it enables the realization of a thermal circulator (FIG. 4l), a three-port or four-port device that can direct radiative heat flow entering any port to the next port. Thermal circulators can have important applications in energy harvesting[116,117]. It has also been shown that a non-reciprocal many-body system, consisting of magneto-optical nanoparticles, can support an equilibrium persistent directional heat current in the absence of a temperature gradient[158]. The circulating nature of this persistent directional heat current is important for constructing thermal circulators and is related to other heat transfer effects, such as the thermal Hall effect[159].

NFRHT also has important implications in energy applications. For instance, although a far-field TPV system has been demonstrated[131], a major challenge is that its power density is inherently limited by the emitter temperature and the associated far-field heat transfer. This challenge can be addressed by using near-field effects[160]. A near-field TPV device (FIG. 4m) with a substantially enhanced power output compared with far-field TPVs was demonstrated[161]. Progress has also been made in enhancing the power density of near-field TPV systems by exploiting both photon tunnelling and electron tunnelling[162,163].

Finally, the concept of photon chemical potential plays an important role in the manipulation of thermal radiation, as we have discussed. For example, a negatively biased semiconductor (that is, with negative photon chemical potential) can have a lower apparent temperature than its thermodynamic temperature and therefore can absorb heat from a surrounding emitter that has a lower thermodynamic temperature. This process is known as negative luminescent refrigeration (FIG. 4n, left). It has been theoretically suggested[164] and experimentally demonstrated[165] that this effect can be significantly enhanced in the near-field regime, opening up possibilities for solid-state refrigeration. A closely related concept is that of positive luminescent refrigeration (FIG. 4n, right), where a positively biased semiconductor can have an apparent temperature much larger than its thermodynamic temperature and can pump heat to a surrounding absorber that has a higher thermodynamic temperature. The combination of near-field heat transfer and positive luminescent refrigeration can potentially lead to large cooling power and performance[166]. However, it remains challenging owing to the need for a semiconductor with high luminescent efficiency.

Active manipulation of heat transfer

The influence of other physical fields on heat transfer can be classified in two categories. One introduces an additional energy source to the system, the other modulates its thermal properties. Thermoelectric effects belong to the first category, as they generate heating or cooling power with an electric current. Thermal convection is a fundamental form of heat transfer, but it can be regarded as a prime example of a multiphysical effect, with thermal energy carried by moving matter. It also belongs to the first category. The second type of influence is based on the sensitivity of the thermal conductivity or emissivity to external fields.

Thermoelectric effects

The study of thermoelectric effects is an active field of research[19,167]. Most work aims to achieve high-efficiency power generation by using the Seebeck effect (a voltage $\Delta V = -\alpha\Delta T$ induced by a temperature difference ΔT, where α is the Seebeck coefficient). The attention on the thermal part is limited to lattice thermal conductivity[168] and Peltier cooling[169].

The lattice thermal conductivity (κ_l) is mostly studied with the aim of reducing it to increase the thermoelectric figure of merit $zT = \alpha^2\sigma T/\kappa$ (REFS[168,169]), where the thermal conductivity (κ) is the sum of the electric (κ_e) and lattice (κ_l) contributions. For metals, κ_e usually obeys the Wiedemann–Franz law: $\kappa_e = L\sigma T$, where L is the Lorenz number and σ the electrical conductivity[170]. Therefore, σ and κ are positively correlated, whereas a low κ_l helps to mitigate the contrasting requirements of a large σ and a small κ for a high zT. The positive correlation between σ and κ is an important issue in the design of multiphysical functionalities that simultaneously manipulate heat and

electric currents. It is favourable when the desired thermal and electric effects are similar, such as in cloaking[40] and camouflaging[41], because the same material can serve as a good conductor or insulator for both fields. However, great efforts are required to design different or even opposite effects for the two fields, such as cloaking the heat flux while focusing an electric current[171,172]. Some materials[173,174], in which the Wiedemann–Franz law is violated upwards[173] or downwards[174], can potentially simplify this design conundrum.

The Joule heating and Peltier cooling effects are practical active approaches to the manipulation of heat using an electric current. Joule heating happens inside the material owing to the inelastic scattering of charge carriers: $g = \mathbf{E}\cdot\mathbf{j} = \alpha\nabla T\cdot\mathbf{j} + j^2/\sigma$, where g is heat generation per unit volume, $\mathbf{E}$ is the electric field, and $\mathbf{j}$ is the electric current density. Modifications to this equation may be required when the device length is comparable to the inelastic mean free path[175,176]. The term $\alpha\nabla T\cdot\mathbf{j}$ comes from the Seebeck effect, and it is counterbalanced by the heat flux carried by the electric current $\Pi\mathbf{j}$, where Π is the Peltier coefficient. Onsager reciprocity leads to the second Thomson relation, $\Pi = \alpha T$, when time-reversal symmetry is preserved[177]. Because of charge conservation ($\nabla\cdot\mathbf{j} = 0$), we have

$$\alpha\nabla T\cdot\mathbf{j} - \nabla\cdot(\Pi\mathbf{j}) = -T\nabla\alpha\cdot\mathbf{j} \qquad (11)$$

which equals zero if the Seebeck coefficient is spatially uniform. Then, Joule heating is $g = j^2/\sigma$ (FIG. 5a). When α is different for materials A and B, there is an additional heat generation at their interface, the Peltier effect. The heat generated per unit area is $q_s = (\Pi_A - \Pi_B)\mathbf{j}\cdot\mathbf{n}$, where $\mathbf{n}$ is the unit vector perpendicular to the interface pointing from A to B (FIG. 5a). When an electric current passes from A to B, it has a cooling effect for $\Pi_A < \Pi_B$. The performance of a Peltier cooler is positively related to zT when the cooler is used for refrigeration, extracting heat from the cold side[177]. However, a high thermal conductivity is preferred for active cooling to aid heat dissipation from the hot side; in this case, a high zT may not be favourable, and some metals are suggested[178]. Joule heating is the governing mechanism of many heaters and most photothermal effects (for example the field of thermo-plasmonics[179] uses plasmonic resonances to convert light into Joule heat). It also hinders the speed and compactness of electronic devices. Combined with Joule heating, the Peltier effect can be used in conductive thermal metamaterials to generate various temperature profiles[180], but these devices require temperature measurement and feedback. By applying thermoelectric modules on the human body, adaptive thermal camouflage can be achieved[181]. Peltier modules can also act as thermal switches[182]. At the nanoscale, thermoelectric rectifiers and transistors have been theoretically proposed to regulate heat using a charge current, based on a nonlinear three-terminal model[183].

A non-uniform Seebeck coefficient can arise if there is a temperature dependence $\alpha(T)$. When this dependence is non-negligible, equation 11 becomes $-T(\mathrm{d}\alpha/\mathrm{d}T)\nabla T\cdot\mathbf{j} = -\tau\nabla T\cdot\mathbf{j}$, where $\tau = T(\mathrm{d}\alpha/\mathrm{d}T) = \mathrm{d}\Pi/\mathrm{d}T - \alpha$ is the Thomson coefficient. This equation describes the Thomson effect used to design thermoelectric modules with graded materials, which in theory can have a

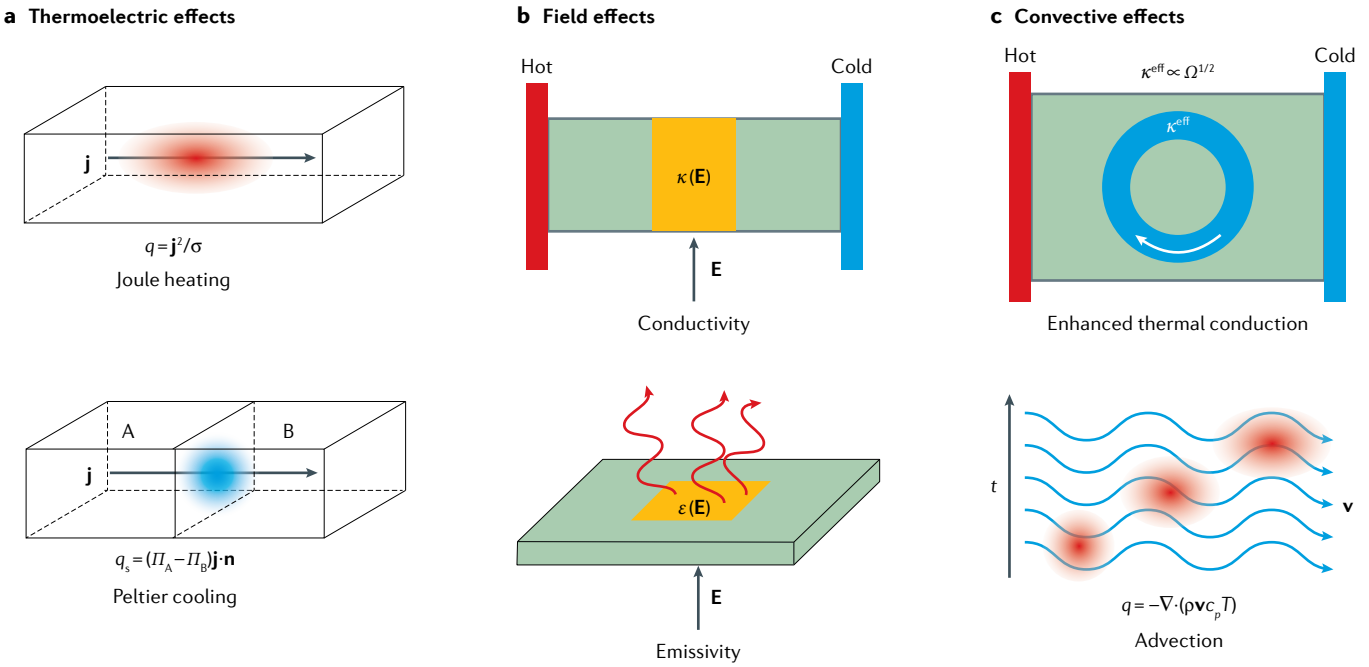

Fig. 5 | **Multiphysical effects for heat transfer manipulation. a** | An electric current can induce Joule heating or Peltier cooling. **b** | Electric (**E**) and magnetic fields can modify the thermal conductivity (κ) and emissivity (ε) of some materials. **c** | Moving matter (set in motion by introducing velocity fields) can enhance the thermal conduction in a solid in contact with the moving fluid or set the temperature field inside it (represented in red) in motion. κ^{eff}, effective thermal conductivity; Π_a and Π_b, Peltier coefficients of materials A and B, respectively; ρ, spectral energy density; σ, electric conductivity; Ω, rotation speed; c_p, specific heat at constant pressure; $\mathbf{j}$, electric current density; $\mathbf{n}$, unit vector normal to the surface; q, heat; q_s, heat generated per unit area; T, temperature; t, time; $\mathbf{v}$, velocity.

much better performance than in the uniform case[184]. The Righi–Leduc effect, or thermal Hall effect, can be induced by a magnetic field or be found in ferromagnets, and generates a heat flux perpendicular to the applied temperature gradient[185]. In addition to electric currents, there is also growing interest in thermal effects induced by or dependent on spin currents[186,187]. In insulators, the magnon Hall effect acting on spin currents also has a thermal counterpart[188].

Field effects. External electric, magnetic or mechanical fields can induce entropy changes and thereby generate or extract heat in some materials through 'caloric' effects[189]. These are often characterized by an isothermal entropy change ΔS. For a strong effect that can be practically used, most studies focus on materials that undergo phase transitions with large entropy changes induced by external fields, including magnetic materials, ferroelectrics and shape-memory alloys. The maximum value of $|\Delta S|$ can be estimated across the phase transition, and good caloric materials have $|\Delta S_{max}|$ around $10\,J\,kg^{-1}\,K^{-1}$. Recently, plastic crystals that act as barocaloric materials[190] were reported to have $|\Delta S_{max}|$ over $300\,J\,kg^{-1}\,K^{-1}$. The caloric effects only work in the transient regime when the external field is temporally changed and are usually reversible when the original field is restored, except for the anomalous electrocaloric effect[191]. Maintaining and using these caloric effects require repeatedly changing the working conditions with working fluids or deformation[192] for refrigeration or heat pumping[193].

External fields can also induce changes in the thermal properties of a material (FIG. 5b). We have already mentioned that temperature dependence and thermoelectric effect can be used to build thermal switches[48]. The field-induced modulation of the thermal conductivity is another important method. It can be achieved through several different mechanisms. First, field-induced phase transitions can be an effective way to introduce fast changes in the thermal conductivity and heat capacity. The metal-to-insulator transition (MIT) of VO_2 is widely studied[194]. It can be triggered or suppressed by an electric field, mechanical strain, hydrogenation and photoexcitation, making it convenient for thermal switches[195] and memories[196]. However, the total thermal conductivity κ of bulk VO_2 is almost constant or even decreases[197] across the MIT[174]. Fortunately, an increase of κ following the Wiedemann–Franz law can be partially restored by introducing tungsten doping[174]. For thin films of VO_2, κ can also increase[195] from ~$4\,W\,m^{-1}\,K^{-1}$ to ~$6\,W\,m^{-1}\,K^{-1}$. Second, the reconfiguration of domain walls in ferroelectric thin films by an electric field can be used to influence the thermal conductivity. At room temperature, the thermal conductivity of a lead zirconate titanate film was reported to decrease upon the application of a gate voltage[198]. Third, for 2D materials it has been proposed that an external electric field can increase the phonon–electron scattering and thereby reduce the lattice thermal conductivity[199].

Electrochemical methods can also achieve reversible modulation of the thermal conductivity, as demonstrated in thin films of $LiCoO_2$ (REF.[200]), graphite[201], black phosphorus[202] and MoS_2 (REFS[203,204]) under lithiation. The effects are often anisotropic. A nanoscale thermal transistor was realized based on the large-ratio and reversible thermal switching in MoS_2 thin films[204]. The underlying mechanisms include lithium-induced disorder, rattler modes and strain. Electrochemically induced 'tri-state' phase transitions have been observed in $SrCoO_x$ (SCO), accompanied by a thermal conductivity increase or decrease up to a factor of ten[205]. The effects of oxygenation and hydrogenation on SCO include disorder as well as changes in lattice parameter, lattice structure and ionic size. In this work, ion gels were used instead of a liquid electrolyte to realize a semi-solid-state device.

In addition to the use of electric fields, many other active methods can be used to influence thermal conduction. At cryogenic temperatures, the lattice thermal conductivity of the diamagnetic semiconductor InSb is reduced by the application of an external magnetic field[206], which is attributed to enhanced phonon–phonon scattering via anharmonic interatomic bonds. A multiferroic thermal diode controllable by modifying the excitations of electric polarization and magnetization with electric or magnetic fields was proposed[207]. Light can trigger a threefold thermal conductivity change in azobenzene polymers through a crystal-to-liquid transition[208]. The effect of strain on the thermal conductivity of nanostructures has also been widely studied[209,210]. A switchable thermal interface has been designed with a solid–liquid hybrid structure, where the combination of copper microposts and water resulted in low thermal resistance under moderate loading pressure[211]. Under high pressure, semiconductor–metal transitions of Si and $Si_{0.991}Ge_{0.009}$ are triggered, leading to substantial thermal conductivity enhancements[212]. Extreme pressure also modifies the phonon dispersion in bulk MoS_2 by enhancing the interlayer interaction, thereby increasing the cross-plane thermal conductivity[213]. At the nanoscale, the van der Waals interaction between boron nanoribbons enhances thermal conduction and is tunable by wetting with various solutions[214]. It is worth noting that these works mostly modulate the heat carrier populations or scattering rates, which are limited to a small spectral range. An interesting work proposed to modulate the displacement amplitudes of vibrations in topologically networked materials[215]. The idea has been demonstrated through hydration of bio-polymers based on squid ring teeth, which changes the crosslinked structure and induces a reversible fourfold change in the thermal conductivity.

The modulation of thermal radiation with external fields has made considerable progress in recent years, thanks to rapid developments in photonics. If the resonant modes of a photonic structure influence its absorption, its thermal emission can be modulated by electric fields, typically through the modified charge carrier density. This mechanism has been demonstrated for quantum wells[21,216], graphene plasmonic resonators[217] and plasmonic metasurfaces[218]. The emissivity spectra of these materials are responsive to a gate voltage, enabling dynamically tunable and polarization-dependent[218] thermal emissions. The idea was extended to the near-field radiative heat transfer between graphene layers[219].

As we mentioned, a gate voltage also modifies the photon chemical potential[164–166]. The electrically induced mechanical deformation of an elastomer membrane with an infrared-reflecting coating has been proposed for adaptive radiative camouflage[220], inspired by the colour-changing capability of cephalopod skin. The use of electric fields was proposed to intercalate Li^+ into $Li_4Ti_5O_{12}$ (REF.[221]), which results in good broadband tunability of the emissivity. A magnetic field can be used to break the detailed balance or Kirchhoff's law. It can also induce a large reduction of near-field heat transfer by suppressing the surface modes in doped semiconductors[222]. Giant thermal magnetoresistance was predicted to enhance the near-field heat transfer in InSb–Ag nanoparticles exposed to orthogonal magnetic fields, owing to the spectral shift of localized surface waves[223]. Such an enhancement was also predicted for near-field heat transfer between graphene sheets at microwave frequencies owing to the field-induced magnetoplasmon zero modes[224].

Static electric and magnetic fields are often uniformly applied; thus, ultraviolet light has been proposed instead to locally modulate the thermal emissivity of an infrared metamaterial with a photosensitive ZnO layer[225]. The modulation speed can be significantly increased by using a visible pulsed laser, which has been used to induce nanosecond pulsed thermal emission from unpatterned silicon and gallium arsenide[226]. The effect of electromagnetic waves is similar to that of a gate voltage that modifies the charge carrier density. Photonic structures can also be deformed by mechanical stimuli. A microelectromechanical system can spatiotemporally reconfigure a metamaterial infrared emitter[227]. A textile made of bimorph fibres coated with carbon nanotubes has been designed for the thermal management of the human body[228]. Its deformation and therefore emission spectrum are sensitive to humidity changes due to sweating. The thermal radiation of some materials is also tunable with chemical stimuli. Biomimetic infrared camouflage coatings have been made from a cephalopod protein that is reconfigurable through the reversible swelling induced by acid vapour[229].

Temperature dependence is another useful mechanism. The MIT of VO_2 is accompanied by a quick drop of emissivity in the mid-infrared[230], as well as decreased near-field heat transfer efficiency[231]. Similar properties are observed in other phase-change materials such as $Ge_2Sb_2Te_5$ (REFS[156,232]). These materials have been proposed to realize a plethora of new effects such as radiative thermal camouflage[156,233], super Stefan–Boltzmann relation[232], radiative thermal rectification[234,235] and zero-differential thermal emittance[232], as well as new devices such as radiative thermal diodes[234], thermal rectifiers[235], thermal homeostasis devices[236] and self-adaptive radiative cooling systems[237].

Convective effects. Convection is a unique and fundamental form of heat transfer. It is impossible to cover it comprehensively here, so we limit the scope of this discussion to works that focus on artificially designed structures for thermal conduction manipulation. Many devices such as thermal exchangers, heat pipes and thermosyphons are thus not discussed, because they directly use thermal convection. A common convective effect on thermal conduction arises from the contact of fluid flow with a solid, and is characterized by the dimensionless Biot number $\mathrm{Bi} = hL_c/\kappa_s$, where L_c is the characteristic length and κ_s is the thermal conductivity of the solid body. The heat transfer coefficient h is related to the heat flux through the surface of the solid as $q_s = h(T_\infty - T)$, where T_∞ is the temperature of the fluid far from the surface. The heat flux generally exists on solid surfaces exposed to air and can influence heat conduction, making the performance of some conductive thermal metamaterials inferior to the ideal case[238]. Fluid flow can also enhance heat transfer (FIG. 5c). For example, the effective thermal conductivity of nanofluids is enhanced by local convective fields induced by Brownian motion[239]. A thermal meta-device was designed with a circulating fluid field[22]; the effective thermal conductivity κ^{eff} of the fluid field is proportional to the square root of the Péclet number $\mathrm{Pe} = \Omega R^2/D$, where Ω is the rotation speed, R is the radius and D is the diffusivity. For more robust control, it was proposed to push $\kappa^{\mathrm{eff}} \to \infty$ (much larger than that of solid materials) by high-speed forced convection.

In thermal convection, thermal energy is carried into or out of the control volume at a rate $-\nabla \cdot (\rho v c_p T)$, where v is the velocity field and c_p is the specific heat at constant pressure[240]. Other factors that need to be considered are viscous dissipation (usually small for laminar flows) and pressure work (negligible for incompressible fluids). Therefore, the heat transfer equation becomes the convection–diffusion equation:

$$\rho c_p \frac{\partial T}{\partial t} = \nabla \cdot (\kappa \nabla T) - \rho c_p v \cdot \nabla T \tag{12}$$

The effects of the velocity field can be considered as a special kind of multiphysical effect on thermal conduction, characterized by the Péclet number $\mathrm{Pe} = |v| L_c/D$. For constant uniform velocity fields, a variable change $r' = r - vt$ restores the diffusive equation, so the temperature field has a moving profile following the background: this is the advection effect (FIG. 5c). For conductive thermal metamaterials, an immediate question is whether the design principles described above are still applicable. The answer is negative. The reason is that although equation 12 is form-invariant[241], the Navier–Stokes equations (momentum equations for incompressible fluids) are not. However, transformation theory applies for thermal convection in porous media with small permeability[242], for which the momentum equation is Darcy's law, which preserves form invariance[243].

Recently, it was proposed to consider equation 12 as a Schrödinger-like equation[244,245], where the convective term is treated as a Hermitian component introduced into a non-Hermitian Hamiltonian. This leads to the realization of anti-parity–time symmetry[246]. One interesting property of an heat transfer system that is anti-parity–time symmetric is that advection is suppressed in the symmetric phase. It could be understood as a cancellation of convective effects inside the field (Pe) with those brought by the adjacent field (Bi). In some

situations, it is favourable for heat transfer in moving matter to be the same as in stationary media for us to predict and control it in the framework of conduction.

Outlook

Heat transfer is a research topic with a very long history. Current research activities are mostly focused on a specific form, either thermal conduction, radiation or convection, at a certain length scale (macroscale or nanoscale), and these activities are usually separated from other research fields.

In this Review, we have tried our best to bring scattered works from different areas under the same umbrella. Some connections are worth noticing. There have been a few attempts to realize thermal cloaking at the nanoscale based on macroscopic designs[57,247]. Transformation theory has been used for the manipulation of radiative signals[34,35,248]. Convection has been used to enhance and cloak conductive heat[22]. Field-induced phase transitions are widely used to modify thermal conduction and radiation at all length scales. There are also theoretical designs of thermal metamaterials aiming at manipulating conductive and radiative heat together[249,250]. Despite all these efforts, a big challenge is still to synergistically use different approaches for more sophisticated and practical heat transfer control. It is difficult to fabricate large-scale nano-engineered phononic structures. Thermoelectric effects and caloric effects are seldom considered as potential methods to modulate heat transfer beyond heating and refrigeration. Building such connections will not only enrich our knowledge but also help to address many multiscale and multiphysical problems, such as heat dissipation in electronic devices and batteries, thermophotovoltaic energy harvesting and thermoelectric temperature regulation.

Finally, we highlight some particularly promising research directions.

Topological effects

The study of the topological properties of materials is an active research field. The phonon Hall effect[251] — a transverse heat flow induced by a magnetic field — was found to be of topological nature[252]. Inspired by their electronic counterparts, phononic topological metamaterials that support topologically protected one-way edge propagation[253] have been demonstrated. However, most work focuses on elastic waves, and the unidirectional propagation of thermal phonons has not been achieved. It is an open question whether we can realize the thermal counterpart of a topological insulator owing to the small wavelength and coherent length of thermal phonons. Besides phonons, heat can also be carried by electrons, magnons and other quasiparticles. Therefore, it is worth studying the potential topological thermal effects induced by these particles and quasiparticles. It is worth noting that many topological insulators and semimetals are thermoelectric materials[254]. Also, chiral heat has been observed in quantum Hall systems[255]. The potential of topological states for improving the thermoelectric performance is being investigated. In magnonic systems, magnon band topology and a thermal magnon Hall effect have attracted intense interest[188,256,257]. Finally, topological heat transport has been predicted in a 2D bosonic Hofstadter lattice[258].

In the rapidly emerging field of topological photonics[259,260], new topological concepts are exploited to design and control the behaviour of photons, leading to remarkable phenomena such as robust unidirectional propagation of light. Ideas from topological photonics may open up new opportunities for photon-based manipulation of heat flux. For example, there is an indication that the persistent heat current in many-body non-reciprocal heat transfer is connected to the presence of one-way edge states[261].

Heat waves. A closely related subject is the wavelike behaviours of heat[262], which is at the base of coherent scattering in NPCs and of local resonances in NPMs and seems to be necessary for any topological effects according to the present theories. At the macroscale, the diffusive Fourier's law indicates that any local perturbation of temperature is instantaneously felt everywhere, which is against causality. Therefore, a rigorous governing equation must contain wavelike terms. These terms are often negligible because of the short relaxation time of the heat carriers. A promising direction to achieve stronger wavelike effects is the second sound[263] (wavelike thermal transport induced by the collective mode of normal phonon–phonon scattering) that was observed in graphite between 85K and 125 K at the micrometre scale[264]. Numerical simulations even predicted the existence of second sound at room temperature in graphene and some other 2D materials[265,266]. This makes it a promising mechanism to realize topological heat transfer[267]. At the macroscale, it was proposed that thermal convection in rotating structures can be regarded as a wavelike component[243].

Quantum effects. As thermal devices reach the nanoscale and atomic scale, the quantum counterparts of conventional thermal devices, such as quantum thermal diodes[268], quantum thermal transistors[269] and quantum heat engines[270–272], are being investigated. An interesting question is whether we can make use of quantum effects, especially quantum coherence, tunnelling and entanglement, to improve the performance of thermal devices or find new mechanisms to control heat. Quantum thermodynamics[273,274] might provide some insightful ideas. Using the trade-off between information and entropy, researchers experimentally demonstrated an on-chip information-powered refrigerator[272], and a spontaneous energy flow from the cold to the hot side in two quantum correlated spin-1/2 systems[275]. It was verified that quantum coherence enables a quantum heat engine to produce more power than its classical counterpart[276]. Although most investigations have shown that quantum effects can be useful in heat manipulation and conversion, these works focused on very small systems (such as a few spins). It is interesting to investigate the scaling of quantum effects with system size, and whether we can make quantum thermal devices at the mesoscopic scale. The exploration of these questions will require accurate control of many-body interactions and good scalability of the

system. The fast development of quantum technologies provides some potential platforms, for example superconducting qubits, ion traps and optomechanical systems.

The fluctuational electrodynamics formalism is widely used to describe near-field heat transfer, which is driven by thermal fluctuations. The same formalism is also used to describe effects related to the quantum fluctuations of electromagnetic waves such as the Casimir effect, in which momentum transfer and hence forces arise between neutral bodies. Thus, there is a strong connection between thermal fluctuation and quantum fluctuation effects. For example, in the presence of quantum fluctuations, phonon heat transfer between two objects separated by a vacuum gap can be achieved[277,278]. The exploration of quantum fluctuations could open up new opportunities for heat transfer manipulation in addition to conduction, convection and radiation.

Published online: 12 March 2021

1. Chen, G. *Nanoscale Energy Transport and Conversion: A Parallel Treatment of Electrons, Molecules, Phonons, and Photons* (Oxford Univ. Press, 2005).
2. Sklan, S. R. & Li, B. Thermal metamaterials: functions and prospects. *Natl Sci. Rev.* **5**, 138–141 (2018).
3. Huang, J.-P. *Theoretical Thermotics: Transformation Thermotics and Extended Theories for Thermal Metamaterials* (Springer, 2020).
4. Li, N. et al. Colloquium: Phononics. Manipulating heat flow with electronic analogs and beyond. *Rev. Mod. Phys.* **84**, 1045–1066 (2012).
5. Li, W. & Fan, S. Nanophotonic control of thermal radiation for energy applications. *Opt. Express* **26**, 15995–16021 (2018).
6. Baranov, D. G. et al. Nanophotonic engineering of far-field thermal emitters. *Nat. Mater.* **18**, 920–930 (2019).
7. Cuevas, J. C. & García-Vidal, F. J. Radiative heat transfer. *ACS Photonics* **5**, 3896–3915 (2018).
8. Fan, C. Z., Gao, Y. & Huang, J. P. Shaped graded materials with an apparent negative thermal conductivity. *Appl. Phys. Lett.* **92**, 251907 (2008).
9. Chen, T., Weng, C.-N. & Chen, J.-S. Cloak for curvilinearly anisotropic media in conduction. *Appl. Phys. Lett.* **93**, 114103 (2008).
10. Narayana, S. & Sato, Y. Heat flux manipulation with engineered thermal materials. *Phys. Rev. Lett.* **108**, 214303 (2012).
This paper reports the experimental realization of a thermal cloak and of other thermal metamaterials with a layered structure.
11. Volz, S. et al. Nanophononics: state of the art and perspectives. *Eur. Phys. J. B* **89**, 15 (2016).
12. Luckyanova, M. N. et al. Coherent phonon heat conduction in superlattices. *Science* **338**, 936–939 (2012).
13. Yu, J.-K., Mitrovic, S., Tham, D., Varghese, J. & Heath, J. R. Reduction of thermal conductivity in phononic nanomesh structures. *Nat. Nanotechnol.* **5**, 718–721 (2010).
This paper describes the control of the thermal conductivity in a 2D nanomesh.
14. Davis, B. L. & Hussein, M. I. Nanophononic metamaterial: thermal conductivity reduction by local resonance. *Phys. Rev. Lett.* **112**, 055505 (2014).
15. Greffet, J. J. et al. Coherent emission of light by thermal sources. *Nature* **416**, 61–64 (2002).
This paper demonstrates far-field thermal radiation manipulation using subwavelength structures.
16. Caldwell, J. D. et al. Low-loss, infrared and terahertz nanophotonics using surface phonon polaritons. *Nanophotonics* **4**, 44–68 (2015).
17. Polder, D. & Van Hove, M. Theory of radiative heat transfer between closely spaced bodies. *Phys. Rev. B* **4**, 3303–3314 (1971).
This paper theoretically describes near-field heat transfer.
18. Volokitin, A. I. & Persson, B. N. J. Near-field radiative heat transfer and noncontact friction. *Rev. Mod. Phys.* **79**, 1291–1329 (2007).
19. He, J. & Tritt, T. M. Advances in thermoelectric materials research: looking back and moving forward. *Science* **357**, eaak9997 (2017).
20. Yoon, H. et al. Reversible phase modulation and hydrogen storage in multivalent VO_2 epitaxial thin films. *Nat. Mater.* **15**, 1113–1119 (2016).
21. Vassant, S. et al. Electrical modulation of emissivity. *Appl. Phys. Lett.* **102**, 081125 (2013).
The paper proposes to modulate thermal emissivity with electric fields.
22. Li, Y. et al. Thermal meta-device in analogue of zero-index photonics. *Nat. Mater.* **18**, 48 (2019).
23. Leonhardt, U. Optical conformal mapping. *Science* **312**, 1777–1780 (2006).
24. Pendry, J. B., Schurig, D. & Smith, D. R. Controlling electromagnetic fields. *Science* **312**, 1780–1782 (2006).
25. Guenneau, S., Amra, C. & Veynante, D. Transformation thermodynamics: cloaking and concentrating heat flux. *Opt. Express* **20**, 8207–8218 (2012).
26. Schittny, R., Kadic, M., Guenneau, S. & Wegener, M. Experiments on transformation thermodynamics: molding the flow of heat. *Phys. Rev. Lett.* **110**, 195901 (2013).
27. Nan, C.-W., Birringer, R., Clarke, D. R. & Gleiter, H. Effective thermal conductivity of particulate composites with interfacial thermal resistance. *J. Appl. Phys.* **81**, 6692–6699 (1997).
28. Sklan, S. R., Bai, X., Li, B. & Zhang, X. Detecting thermal cloaks via transient effects. *Sci. Rep.* **6**, 32915 (2016).
29. Han, T. et al. Theoretical realization of an ultra-efficient thermal-energy harvesting cell made of natural materials. *Energy Environ. Sci.* **6**, 3537–3541 (2013).
30. Shen, X., Jiang, C., Li, Y. & Huang, J. Thermal metamaterial for convergent transfer of conductive heat with high efficiency. *Appl. Phys. Lett.* **109**, 201906 (2016).
31. Hu, R. et al. Binary thermal encoding by energy shielding and harvesting units. *Phys. Rev. Appl.* **10**, 054032 (2018).
32. Li, J. et al. Doublet thermal metadevice. *Phys. Rev. Appl.* **11**, 044021 (2019).
33. Hu, R. et al. Illusion thermotics. *Adv. Mater.* **30**, 1707237 (2018).
34. Li, Y., Bai, X., Yang, T., Luo, H. & Qiu, C.-W. Structured thermal surface for radiative camouflage. *Nat. Commun.* **9**, 273 (2018).
35. Peng, Y.-G., Li, Y., Cao, P.-C., Zhu, X.-F. & Qiu, C.-W. 3D Printed meta-helmet for wide-angle thermal camouflages. *Adv. Funct. Mater.* **30**, 2002061 (2020).
36. Shang, J., Tian, B. Y., Jiang, C. R. & Huang, J. P. Digital thermal metasurface with arbitrary infrared thermogram. *Appl. Phys. Lett.* **113**, 261902 (2018).
37. Gomory, F. et al. Experimental realization of a magnetic cloak. *Science* **335**, 1466–1468 (2012).
38. Xu, H., Shi, X., Gao, F., Sun, H. & Zhang, B. Experimental demonstration of an ultrathin three-dimensional thermal cloak. *Phys. Rev. Lett.* **112**, 054301 (2014).
This paper and the one below by Han et al. present the experimental realization of thermal cloaks with only two layers of natural materials.
39. Han, T. et al. Experimental demonstration of a bilayer thermal cloak. *Phys. Rev. Lett.* **112**, 054302 (2014).
40. Ma, Y., Liu, Y., Raza, M., Wang, Y. & He, S. Experimental demonstration of a multiphysics cloak: manipulating heat flux and electric current simultaneously. *Phys. Rev. Lett.* **113**, 205501 (2014).
41. Yang, T. et al. Invisible sensor: simultaneous sensing and camouflaging in multiphysical fields. *Adv. Mater.* **27**, 7752–7758 (2015).
42. Han, T., Bai, X., Thong, J. T. L., Li, B. & Qiu, C.-W. Full control and manipulation of heat signatures: cloaking, camouflage and thermal metamaterials. *Adv. Mater.* **26**, 1731–1734 (2014).
43. Xu, L., Yang, S. & Huang, J. Thermal transparency induced by periodic interparticle interaction. *Phys. Rev. Appl.* **11**, 034056 (2019).
44. Xu, L., Yang, S. & Huang, J. Passive metashells with adaptive thermal conductivities: chameleonlike behaviour and its origin. *Phys. Rev. Appl.* **11**, 054071 (2019).
45. Han, T. et al. Full-parameter omnidirectional thermal metadevices of anisotropic geometry. *Adv. Mater.* **30**, 1804019 (2018).
46. Fujii, G. & Akimoto, Y. Topology-optimized thermal carpet cloak expressed by an immersed-boundary level-set method via a covariance matrix adaptation evolution strategy. *Int. J. Heat Mass Transf.* **137**, 1312–1322 (2019).
47. Zheng, X. & Li, B. Effect of interfacial thermal resistance in a thermal cloak. *Phys. Rev. Appl.* **13**, 024071 (2020).
48. Wehmeyer, G., Yabuki, T., Monachon, C., Wu, J. & Dames, C. Thermal diodes, regulators, and switches: Physical mechanisms and potential applications. *Appl. Phys. Rev.* **4**, 041304 (2017).
49. Li, Y. et al. Temperature-dependent transformation thermotics: from switchable thermal cloaks to macroscopic thermal diodes. *Phys. Rev. Lett.* **115**, 195503 (2015).
50. Sklan, S. R. & Li, B. A unified approach to nonlinear transformation materials. *Sci. Rep.* **8**, 4436 (2018).
51. Li, Y., Shen, X., Huang, J. & Ni, Y. Temperature-dependent transformation thermotics for unsteady states: Switchable concentrator for transient heat flow. *Phys. Lett. A* **380**, 1641–1647 (2016).
52. Shen, X., Li, Y., Jiang, C., Ni, Y. & Huang, J. Thermal cloak-concentrator. *Appl. Phys. Lett.* **109**, 031907 (2016).
53. Shen, X., Li, Y., Jiang, C. & Huang, J. Temperature trapping: energy-free maintenance of constant temperatures as ambient temperature gradients change. *Phys. Rev. Lett.* **117**, 055501 (2016).
54. Hao, M., Li, J., Park, S., Moura, S. & Dames, C. Efficient thermal management of Li-ion batteries with a passive interfacial thermal regulator based on a shape memory alloy. *Nat. Energy* **3**, 899–906 (2018).
55. Kang, S. et al. Temperature-responsive thermal metamaterials enabled by modular design of thermally tunable unit cells. *Int. J. Heat Mass Transf.* **130**, 469–482 (2019).
56. Zhao, Y. et al. Engineering the thermal conductivity along an individual silicon nanowire by selective helium ion irradiation. *Nat. Commun.* **8**, 15919 (2017).
57. Choe, H. S. et al. Ion write microthermotics: programing thermal metamaterials at the microscale. *Nano Lett.* **19**, 3830–3837 (2019).
58. Maldovan, M. Sound and heat revolutions in phononics. *Nature* **503**, 209–217 (2013).
59. Verdier, M., Anufriev, R., Ramiere, A., Termentzidis, K. & Lacroix, D. Thermal conductivity of phononic membranes with aligned and staggered lattices of holes at room and low temperatures. *Phys. Rev. B* **95**, 205438 (2017).
60. Anufriev, R., Ramiere, A., Maire, J. & Nomura, M. Heat guiding and focusing using ballistic phonon transport in phononic nanostructures. *Nat. Commun.* **8**, 15505 (2017).
61. Anufriev, R., Gluchko, S., Volz, S. & Nomura, M. Quasi-ballistic heat conduction due to Lévy phonon flights in silicon nanowires. *ACS Nano* **12**, 11928–11935 (2018).
62. Costescu, R., Cahill, D. G., Fabreguette, F., Sechrist, Z. & George, S. Ultra-low thermal conductivity in W/Al_2O_3 nanolaminates. *Science* **303**, 989–990 (2004).
63. Simkin, M. V. & Mahan, G. D. Minimum thermal conductivity of superlattices. *Phys. Rev. Lett.* **84**, 927 (2000).
64. Cleland, A. N., Schmidt, D. R. & Yung, C. S. Thermal conductance of nanostructured phononic crystals. *Phys. Rev. B* **64**, 172301 (2001).
65. Ravichandran, J. et al. Crossover from incoherent to coherent phonon scattering in epitaxial oxide superlattices. *Nat. Mater.* **13**, 168 (2014).
66. Tang, J. et al. Holey silicon as an efficient thermoelectric material. *Nano Lett.* **10**, 4279–4283 (2010).
67. Hopkins, P. E. et al. Reduction in the thermal conductivity of single crystalline silicon by phononic crystal patterning. *Nano Lett.* **11**, 107–112 (2010).

68. He, Y., Donadio, D., Lee, J.-H., Grossman, J. C. & Galli, G. Thermal transport in nanoporous silicon: interplay between disorder at mesoscopic and atomic scales. *ACS Nano* **5**, 1839–1844 (2011).
69. Zen, N., Puurtinen, T. A., Isotalo, T. J., Chaudhuri, S. & Maasilta, I. J. Engineering thermal conductance using a two-dimensional phononic crystal. *Nat. Commun.* **5**, 3435 (2014).
70. Alaie, S. et al. Thermal transport in phononic crystals and the observation of coherent phonon scattering at room temperature. *Nat. Commun.* **6**, 7228 (2015).
71. Lim, J. et al. Simultaneous thermoelectric property measurement and incoherent phonon transport in holey silicon. *ACS Nano* **10**, 124–132 (2015).
72. Nakagawa, J., Kage, Y., Hori, T., Shiomi, J. & Nomura, M. Crystal structure dependent thermal conductivity in two-dimensional phononic crystal nanostructures. *Appl. Phys. Lett.* **107**, 023104 (2015).
73. Nomura, M., Nakagawa, J., Sawano, K., Maire, J. & Volz, S. Thermal conduction in Si and SiGe phononic crystals explained by phonon mean free path spectrum. *Appl. Phys. Lett.* **109**, 173104 (2016).
74. Lee, J. et al. Investigation of phonon coherence and backscattering using silicon nanomeshes. *Nat. Commun.* **8**, 14054 (2017).
75. Maire, J. et al. Heat conduction tuning by wave nature of phonons. *Sci. Adv.* **3**, e1700027 (2017).
76. Yang, L., Yang, N. & Li, B. Reduction of thermal conductivity by nanoscale 3D phononic crystal. *Sci. Rep.* **3**, 1143 (2013).
77. Yang, L., Yang, N. & Li, B. Extreme low thermal conductivity in nanoscale 3D Si phononic crystal with spherical pores. *Nano Lett.* **14**, 1734–1738 (2014).
78. Yang, L., Chen, J., Yang, N. & Li, B. Significant reduction of graphene thermal conductivity by phononic crystal structure. *Int. J. Heat Mass Transf.* **91**, 428–432 (2015).
79. Dechaumphai, E. & Chen, R. Thermal transport in phononic crystals: the role of zone folding effect. *J. Appl. Phys.* **111**, 073508 (2012).
80. Jain, A., Yu, Y.-J. & McGaughey, A. J. Phonon transport in periodic silicon nanoporous films with feature sizes greater than 100 nm. *Phys. Rev. B* **87**, 195301 (2013).
81. Ravichandran, N. K. & Minnich, A. J. Coherent and incoherent thermal transport in nanomeshes. *Phys. Rev. B* **89**, 205432 (2014).
82. Ding, D., Yin, X. & Li, B. Sensing coherent phonons with two-photon interference. *N. J. Phys.* **20**, 023008 (2018).
83. Honarvar, H. & Hussein, M. I. Two orders of magnitude reduction in silicon membrane thermal conductivity by resonance hybridizations. *Phys. Rev. B* **97**, 195413 (2018).
84. Hussein, M. I. & Honarvar, H. in *Handbook of Materials Modeling: Applications. Current and Emerging Materials* (eds Andreoni, W. & Yip, S.) 953–973 (Springer, 2020).
85. Liu, Y. Y. et al. An efficient mechanism for enhancing the thermoelectricity of nanoribbons by blocking phonon transport in 2D materials. *J. Phys. Condens. Matter* **30**, 275701 (2018).
86. Giri, A. & Hopkins, P. E. Giant reduction and tunability of the thermal conductivity of carbon nanotubes through low-frequency resonant modes. *Phys. Rev. B* **98**, 45421 (2018).
87. Hussein, M. I., Tsai, C.-N. & Honarvar, H. Thermal conductivity reduction in a nanophononic metamaterial versus a nanophononic crystal: a review and comparative analysis. *Adv. Funct. Mater.* **30**, 1906718 (2020).
88. Anufriev, R., Yanagisawa, R. & Nomura, M. Aluminium nanopillars reduce thermal conductivity of silicon nanobeams. *Nanoscale* **9**, 15083–15088 (2017).
89. Honarvar, H. & Hussein, M. I. Spectral energy analysis of locally resonant nanophononic metamaterials by molecular simulations. *Phys. Rev. B* **93**, 081412 (2016).
90. Ma, D. et al. Nano-cross-junction effect on phonon transport in silicon nanowire cages. *Phys. Rev. B* **94**, 165434 (2016).
91. Xiong, S. et al. Blocking phonon transport by structural resonances in alloy-based nanophononic metamaterials leads to ultralow thermal conductivity. *Phys. Rev. Lett.* **117**, 025503 (2016).
92. Anufriev, R. & Nomura, M. Heat conduction engineering in pillar-based phononic crystals. *Phys. Rev. B* **95**, 155432 (2017).
93. Wei, Z., Yang, J., Bi, K. & Chen, Y. Phonon transport properties in pillared silicon film. *J. Appl. Phys.* **118**, 155103 (2015).
94. Chen, J., Zhang, G. & Li, B. Phonon coherent resonance and its effect on thermal transport in core–shell nanowires. *J. Chem. Phys.* **135**, 104508 (2011).
95. Howell, J. R., Siegel, R. & Mengüc, M. P. *Thermal Radiation Heat Transfer* (CRC, 2011).
96. Modest, M. F. *Radiative Heat Transfer* (Elsevier, 2013).
97. Kittel, C. & Kroemer, H. *Thermal Physics* (Freeman, 1980).
98. Cornelius, C. M. & Dowling, J. P. Modification of Planck blackbody radiation by photonic band-gap structures. *Phys. Rev. A* **59**, 4736–4746 (1999).
99. Lin, S. Y. et al. Enhancement and suppression of thermal emission by a three-dimensional photonic crystal. *Phys. Rev. B* **62**, R2243–R2246 (2000).
100. Noda, S. Conversion of broadband to narrowband thermal emission through energy recycling. *Nat. Photonics* **6**, 535–539 (2012).
101. Celanovic, I. Enabling high-temperature nanophotonics for energy applications. *Proc. Natl Acad. Sci. USA* **109**, 2280–2285 (2012).
102. Dahan, N., Niv, A., Biener, G., Kleiner, V. & Hasman, E. Space-variant polarization manipulation of a thermal emission by a SiO_2 subwavelength grating supporting surface phonon-polaritons. *Appl. Phys. Lett.* **86**, 191102 (2005).
103. Liu, X. et al. Taming the blackbody with infrared metamaterials as selective thermal emitters. *Phys. Rev. Lett.* **107**, 045901 (2011).
104. Dyachenko, P. N. et al. Controlling thermal emission with refractory epsilon-near-zero metamaterials via topological transitions. *Nat. Commun.* **7**, 11809 (2016).
105. Li, W., Shi, Y., Chen, Z. & Fan, S. Photonic thermal management of coloured objects. *Nat. Commun.* **9**, 4240 (2018).
106. Hurtado, F. et al. Super-Planckian far-field radiative heat transfer. *Phys. Rev. B* **97**, 045408 (2018).
107. Thompson et al. Hundred-fold enhancement in far-field radiative heat transfer over the blackbody limit. *Nature* **561**, 216 (2018).
108. Shin, Sunmi, Elzouka, M., Prasher, R. & Chen, R. Far-field coherent thermal emission from polaritonic resonance in individual anisotropic nanoribbons. *Nat. Commun.* **10**, 1377 (2019).
109. Yu, Z. et al. Enhancing far-field thermal emission with thermal extraction. *Nat. Commun.* **4**, 1730 (2013).
110. Ding, D., Kim, T. & Minnich, A. J. Active thermal extraction of near-field thermal radiation. *Phys. Rev. B* **93**, 081402 (2016).
111. Messina, R., Ben-Abdallah, P., Guizal, B., Antezza, M. & Biehs, S.-A. Hyperbolic waveguide for long-distance transport of near-field heat flux. *Phys. Rev. B* **94**, 104301 (2016).
112. Wurfel, P. The chemical potential of radiation. *J. Phys. C* **15**, 3967–3985 (1982).
113. Buddhiraju, S., Li, W. & Fan, S. Photonic refrigeration from time-modulated thermal emission. *Phys. Rev. Lett.* **124**, 077402 (2020).
114. Khandekar, C., Pick, A., Johnson, S. G. & Rodriguez, A. W. Radiative heat transfer in nonlinear Kerr media. *Phys. Rev. B* **91**, 115406 (2015).
115. Khandekar, C., Lin, Z. & Rodriguez, A. W. Thermal radiation from optically driven Kerr ($\chi(3)$) photonic cavities. *Appl. Phys. Lett.* **106**, 151109 (2015).
116. Landsberg, P. T. & Tonge, G. Thermodynamic energy conversion efficiencies. *J. Appl. Phys.* **51**, R1–R20 (1980).
117. Buddhiraju, S., Santhanam, P. & Fan, S. Thermodynamic limits of energy harvesting from outgoing thermal radiation. *Proc. Natl Acad. Sci. USA* **115**, E3609–E3615 (2018).
118. Zhu, L. & Fan, S. Near-complete violation of detailed balance in thermal radiation. *Phys. Rev. B* **90**, 220301 (2014).
119. Rephaeli, E., Raman, A. & Fan, S. Ultrabroadband photonic structures to achieve high-performance daytime radiative cooling. *Nano Lett.* **13**, 1457–1461 (2013).
120. Raman, A., Anoma, M. A., Zhu, L., Rephaeli, E. & Fan, S. Passive radiative cooling below ambient air temperature under direct sunlight. *Nature* **515**, 540 (2014).
This paper reports the experimental demonstration of daytime radiative cooling.
121. Zhai, Y. et al. Scalable-manufactured randomized glass–polymer hybrid metamaterial for daytime radiative cooling. *Science* **355**, 1062–1066 (2017).
122. Goldstein, E. A., Raman, A. P. & Fan, S. Sub-ambient non-evaporative fluid cooling with the sky. *Nat. Energy* **2**, 1–7 (2017).
123. Mandal, J. et al. Hierarchically porous polymer coatings for highly efficient passive daytime radiative cooling. *Science* **362**, 315–319 (2018).
124. Li, T. et al. A radiative cooling structural material. *Science* **364**, 760–763 (2019).
125. Li, W., Buddhiraju, S. & Fan, S. Thermodynamic limits for simultaneous energy harvesting from the hot sun and cold outer space. *Light Sci. Appl.* **9**, 68 (2020).
126. Li, W. & Fan, S. Radiative cooling: harvesting the coldness of the Universe. *Opt. Photon. N.* **30**, 32–39 (2019).
127. Swanson, R. M. A proposed thermophotovoltaic solar energy conversion system. *Proc. IEEE* **67**, 446–447 (1979).
This paper proposes the solar thermophotovoltaic concept for thermal radiation energy harvesting.
128. Harder, N.-P. & Würfel, P. Theoretical limits of thermophotovoltaic solar energy conversion. *Semicond. Sci. Technol.* **18**, S151–S157 (2003).
129. Lenert, A. et al. A nanophotonic solar thermophotovoltaic device. *Nat. Nanotechnol.* **9**, 126 (2014).
130. Bierman, D. et al. Enhanced photovoltaic energy conversion using thermally based spectral shaping. *Nat. Energy* **1**, 16068 (2016).
131. Omair, Z. et al. Ultraefficient thermophotovoltaic power conversion by band-edge spectral filtering. *Proc. Natl Acad. Sci. USA* **116**, 15356–15361 (2019).
132. Ilic, O. et al. Tailoring high-temperature radiation and the resurrection of the incandescent source. *Nat. Nanotechnol.* **11**, 320 (2016).
133. Leroy, A. et al. Combined selective emitter and filter for high performance incandescent lighting. *Appl. Phys. Lett.* **111**, 094103 (2017).
134. Shi, Y., Li, W., Raman, A. & Fan, S. Optimization of multilayer optical films with a memetic algorithm and mixed integer programming. *ACS Photonics* **5**, 684–691 (2018).
135. Basu, S., Zhang, Z. & Fu, C. Review of near-field thermal radiation and its application to energy conversion. *Int. J. Energy Res.* **33**, 1203–1232 (2009).
136. Shen, S., Narayanaswamy, A. & Chen, G. Surface phonon polaritons mediated energy transfer between nanoscale gaps. *Nano Lett.* **9**, 2909–2913 (2009).
137. Kim, K. et al. Radiative heat transfer in the extreme near field. *Nature* **528**, 387–391 (2015).
138. Song, B. et al. Radiative heat conductances between dielectric and metallic parallel plates with nanoscale gaps. *Nat. Nanotechnol.* **11**, 509–514 (2016).
139. St-Gelais, R., Zhu, L. X., Fan, S. H. & Lipson, M. Near-field radiative heat transfer between parallel structures in the deep subwavelength regime. *Nat. Nanotechnol.* **11**, 515–519 (2016).
140. Pendry, J. B. Radiative exchange of heat between nanostructures. *J. Phys. Condens. Matter* **11**, 6621 (1999).
141. Mulet, J., Joulain, K., Carminati, R. & Greffet, J. Enhanced radiative heat transfer at nanometric distances. *Microscale Thermophys. Eng.* **6**, 209–222 (2002).
142. Fu, C. & Zhang, Z. Nanoscale radiation heat transfer for silicon at different doping levels. *Int. J. Heat Mass Transf.* **49**, 1703–1718 (2006).
143. Basu, S. & Zhang, Z. Maximum energy transfer in near-field thermal radiation at nanometer distances. *J. Appl. Phys.* **105**, 093535 (2009).
144. Hurtado, V., Vidal, F., Fan, S. & Cuevas, J. Enhancing near-field radiative heat transfer with Si-based metasurfaces. *Phys. Rev. Lett.* **118**, 203901 (2017).
145. Rodriguez, A. et al. Frequency-selective near-field radiative heat transfer between photonic crystal slabs: a computational approach for arbitrary geometries and materials. *Phys. Rev. Lett.* **107**, 114302 (2011).
146. Dai, J., Dyakov, S. A. & Yan, M. Enhanced near-field radiative heat transfer between corrugated metal plates: role of spoof surface plasmon polaritons. *Phys. Rev. B* **92**, 035419 (2015).
147. Iizuka, H. & Fan, S. Significant enhancement of near-field electromagnetic heat transfer in a multilayer structure through multiple surface-states coupling. *Phys. Rev. Lett.* **120**, 063901 (2018).
148. Guo, Y., Cortes, C. L., Molesky, S. & Jacob, Z. Broadband super-Planckian thermal emission from hyperbolic metamaterials. *Appl. Phys. Lett.* **101**, 131106 (2012).
149. Miller, O. D., Steven, G. J. & Rodriguez, A. W. Shape-independent limits to near-field radiative heat transfer. *Phys. Rev. Lett.* **115**, 204302 (2015).

150. Shim, H., Fan, L., Johnson, S. G. & Miller, O. D. Fundamental limits to near-field optical response over any bandwidth. *Phys. Rev. X* **9**, 011043 (2019).
151. Molesky, S., Venkataram, P. S., Jin, W. & Rodriguez, A. W. Fundamental limits to radiative heat transfer: theory. *Phys. Rev. B* **101**, 035408 (2020).
152. Jin, W., Molesky, S., Lin, Z. & Rodriguez, A. W. Material scaling and frequency-selective enhancement of near-field radiative heat transfer for lossy metals in two dimensions via inverse design. *Phys. Rev. B* **99**, 041403 (2019).
153. Otey, Clayton, Lau, W. T. & Fan, S. Thermal rectification through vacuum. *Phys. Rev. Lett.* **104**, 154301 (2010).
154. Yang, Y., Basu, S. & Wang, L. Radiation-based near-field thermal rectification with phase transition materials. *Appl. Phys. Lett.* **103**, 163101 (2013).
155. Fiorino, A. et al. A thermal diode based on nanoscale thermal radiation. *ACS Nano* **12**, 5774–5779 (2018).
156. Qu, Y. et al. Thermal camouflage based on the phase-changing material GST. *Light Sci. Appl.* **7**, 26 (2018).
157. Ben-Abdallah, P. & Biehs, S. A. Near-field thermal transistor. *Phys. Rev. Lett.* **112**, 044301 (2014).
158. Zhu, L. & Fan, S. Persistent directional current at equilibrium in nonreciprocal many-body near field electromagnetic heat transfer. *Phys. Rev. Lett.* **117**, 134303 (2016).
159. Ben-Abdallah, P. Photon thermal Hall effect. *Phys. Rev. Lett.* **116**, 084301 (2016).
160. Basu, S., Chen, Y. B. & Zhang, Z. M. Microscale radiation in thermophotovoltaic devices — a review. *Int. J. Energy Res.* **31**, 689–716 (2007).
161. Anthony et al. Nanogap near-field thermophotovoltaics. *Nat. Nanotechnol.* **13**, 806 (2018).
162. Datas, A. & Vaillon, R. Thermionic-enhanced near-field thermophotovoltaics. *Nano Energy* **61**, 10–17 (2019).
163. Davids, P. S. et al. Electrical power generation from moderate-temperature radiative thermal sources. *Science* **367**, 1341–1345 (2020).
164. Chen, K., Santhanam, P. & Fan, S. Near-field enhanced negative luminescent refrigeration. *Phys. Rev. Appl.* **6**, 024014 (2016).
165. Zhu, L. et al. Near-field photonic cooling through control of the chemical potential of photons. *Nature* **566**, 239 (2019).
166. Chen, K., Santhanam, P., Sandhu, S., Zhu, L. & Fan, S. Heat-flux control and solid-state cooling by regulating chemical potential of photons in near-field electromagnetic heat transfer. *Phys. Rev. B* **91**, 134301 (2015).
167. Zhou, X. et al. Routes for high-performance thermoelectric materials. *Mater. Today* **21**, 974–988 (2018).
168. Snyder, G. J. & Toberer, E. S. Complex thermoelectric materials. *Nat. Mater.* **7**, 105–114 (2008).
169. Ziabari, A., Zebarjadi, M., Vashaee, D. & Shakouri, A. Nanoscale solid-state cooling: a review. *Rep. Prog. Phys.* **79**, 095901 (2016).
170. Tian, Z., Lee, S. & Chen, G. Heat transfer in thermoelectric materials and devices. *J. Heat Transf.* **135**, 061605–061605–15 (2013).
171. Moccia, M., Castaldi, G., Savo, S., Sato, Y. & Galdi, V. Independent manipulation of heat and electrical current via bifunctional metamaterials. *Phys. Rev. X* **4**, 021025 (2014).
This paper reports the fabrication of multiphysical metamaterials with opposite effects on heat and electrical currents.
172. Lan, C., Bi, K., Fu, X., Li, B. & Zhou, J. Bifunctional metamaterials with simultaneous and independent manipulation of thermal and electric fields. *Opt. Express* **24**, 23072–23080 (2016).
173. Crossno, J. et al. Observation of the Dirac fluid and the breakdown of the Wiedemann–Franz law in graphene. *Science* **351**, 1058–1061 (2016).
174. Lee, S. et al. Anomalously low electronic thermal conductivity in metallic vanadium dioxide. *Science* **355**, 371–374 (2017).
175. Pop, E. Energy dissipation and transport in nanoscale devices. *Nano Res.* **3**, 147–169 (2010).
176. Dubi, Y. & Di Ventra, M. Colloquium: Heat flow and thermoelectricity in atomic and molecular junctions. *Rev. Mod. Phys.* **83**, 131–155 (2011).
177. Rowe, D. M. *Thermoelectrics Handbook: Macro to Nano* (CRC, 2018).
178. Adams, M. J., Verosky, M., Zebarjadi, M. & Heremans, J. P. Active Peltier coolers based on correlated and magnon-drag. *Met. Phys. Rev. Appl.* **11**, 054008 (2019).
179. Baffou, G. & Quidant, R. Thermo-plasmonics: using metallic nanostructures as nano-sources of heat. *Laser Photonics Rev.* **7**, 171–187 (2013).
180. Nguyen, D. M., Xu, H., Zhang, Y. & Zhang, B. Active thermal cloak. *Appl. Phys. Lett.* **107**, 121901 (2015).
181. Hong, S., Shin, S. & Chen, R. An adaptive and wearable thermal camouflage device. *Adv. Funct. Mater.* **30**, 1909788 (2020).
182. Adams, M. J., Verosky, M., Zebarjadi, M. & Heremans, J. P. High switching ratio variable-temperature solid-state thermal switch based on thermoelectric effects. *Int. J. Heat Mass Transf.* **134**, 114–118 (2019).
183. Jiang, J.-H., Kulkarni, M., Segal, D. & Imry, Y. Phonon thermoelectric transistors and rectifiers. *Phys. Rev. B* **92**, 045309 (2015).
184. Snyder, G. J., Toberer, E. S., Khanna, R. & Seifert, W. Improved thermoelectric cooling based on the Thomson effect. *Phys. Rev. B* **86**, 045202 (2012).
185. Li, X. et al. Anomalous Nernst and Righi–Leduc effects in Mn_3Sn: Berry curvature and entropy flow. *Phys. Rev. Lett.* **119**, 056601 (2017).
186. Bauer, G. E. W., Saitoh, E. & van Wees, B. J. Spin caloritronics. *Nat. Mater.* **11**, 391–399 (2012).
187. Boona, S. R., Myers, R. C. & Heremans, J. P. Spin caloritronics. *Energy Environ. Sci.* **7**, 885–910 (2014).
188. Ideue, T., Kurumaji, T., Ishiwata, S. & Tokura, Y. Giant thermal Hall effect in multiferroics. *Nat. Mater.* **16**, 797–802 (2017).
189. Moya, X., Kar-Narayan, S. & Mathur, N. D. Caloric materials near ferroic phase transitions. *Nat. Mater.* **13**, 439–450 (2014).
190. Li, B. et al. Colossal barocaloric effects in plastic crystals. *Nature* **567**, 506 (2019).
191. Qian, X., Yang, T., Zhang, T., Chen, L.-Q. & Zhang, Q. M. Anomalous negative electrocaloric effect in a relaxor/normal ferroelectric polymer blend with controlled nano- and meso-dipolar couplings. *Appl. Phys. Lett.* **108**, 142902 (2016).
192. Ma, R. et al. Highly efficient electrocaloric cooling with electrostatic actuation. *Science* **357**, 1130–1134 (2017).
193. Kitanovski, A., Plaznik, U., Tomc, U. & Poredoš, A. Present and future caloric refrigeration and heat-pump technologies. *Int. J. Refrig.* **57**, 288–298 (2015).
194. Liu, K., Lee, S., Yang, S., Delaire, O. & Wu, J. Recent progresses on physics and applications of vanadium dioxide. *Mater. Today* **21**, 875–896 (2018).
195. Oh, D.-W., Ko, C., Ramanathan, S. & Cahill, D. G. Thermal conductivity and dynamic heat capacity across the metal–insulator transition in thin film VO_2. *Appl. Phys. Lett.* **96**, 151906 (2010).
196. Xie, R. et al. An electrically tuned solid-state thermal memory based on metal–insulator transition of single-crystalline VO_2 nanobeams. *Adv. Funct. Mater.* **21**, 1602–1607 (2011).
197. Chen, J. et al. Investigation of the thermal conductivities across metal–insulator transition in polycrystalline VO_2. *Chin. Sci. Bull.* **57**, 3393–3396 (2012).
198. Ihlefeld, J. F. et al. Room-temperature voltage tunable phonon thermal conductivity via reconfigurable interfaces in ferroelectric thin films. *Nano Lett.* **15**, 1791–1795 (2015).
199. Yue, S.-Y., Yang, R. & Liao, B. Controlling thermal conductivity of two-dimensional materials via externally induced phonon–electron interaction. *Phys. Rev. B* **100**, 115408 (2019).
200. Cho, J. et al. Electrochemically tunable thermal conductivity of lithium cobalt oxide. *Nat. Commun.* **5**, 4035 (2014).
201. Qian, X., Gu, X., Dresselhaus, M. S. & Yang, R. Anisotropic tuning of graphite thermal conductivity by lithium intercalation. *J. Phys. Chem. Lett.* **7**, 4744–4750 (2016).
202. Kang, J. S., Ke, M. & Hu, Y. Ionic intercalation in two-dimensional van der Waals materials: in situ characterization and electrochemical control of the anisotropic thermal conductivity of black phosphorus. *Nano Lett.* **17**, 1431–1438 (2017).
203. Zhu, G. et al. Tuning thermal conductivity in molybdenum disulfide by electrochemical intercalation. *Nat. Commun.* **7**, 13211 (2016).
204. Sood, A. et al. An electrochemical thermal transistor. *Nat. Commun.* **9**, 4510 (2018).
205. Lu, Q. et al. Bi-directional tuning of thermal transport in $SrCoO_x$ with electrochemically induced phase transitions. *Nat. Mater.* **19**, 655–662 (2020).
206. Jin, H. et al. Phonon-induced diamagnetic force and its effect on the lattice thermal conductivity. *Nat. Mater.* **14**, 601–606 (2015).
207. Chotorlishvili, L., Etesami, S. R., Berakdar, J., Khomeriki, R. & Ren, J. Electromagnetically controlled multiferroic thermal diode. *Phys. Rev. B* **92**, 134424 (2015).
208. Shin, J. et al. Light-triggered thermal conductivity switching in azobenzene polymers. *Proc. Natl Acad. Sci. USA* **116**, 5973–5978 (2019).
209. Li, X., Maute, K., Dunn, M. L. & Yang, R. Strain effects on the thermal conductivity of nanostructures. *Phys. Rev. B* **81**, 245318 (2010).
210. Wei, N., Xu, L., Wang, H.-Q. & Zheng, J.-C. Strain engineering of thermal conductivity in graphene sheets and nanoribbons: a demonstration of magic flexibility. *Nanotechnology* **22**, 105705 (2011).
211. Jia, Y. & Ju, Y. S. Solid-liquid hybrid thermal interfaces for low-contact pressure thermal switching. *J. Heat Transf.* **136**, 074503 (2014).
212. Hohensee, G. T., Fellinger, M. R., Trinkle, D. R. & Cahill, D. G. Thermal transport across high-pressure semiconductor–metal transition in Si and $Si_{0.991}Ge_{0.009}$. *Phys. Rev. B* **91**, 205104 (2015).
213. Meng, X. et al. Thermal conductivity enhancement in MoS_2 under extreme strain. *Phys. Rev. Lett.* **122**, 155901 (2019).
214. Yang, J. et al. Enhanced and switchable nanoscale thermal conduction due to van der Waals interfaces. *Nat. Nanotechnol.* **7**, 91–95 (2012).
215. Tomko, J. A. et al. Tunable thermal transport and reversible thermal conductivity switching in topologically networked bio-inspired materials. *Nat. Nanotechnol.* **13**, 959–964 (2018).
216. Inoue, T., Zoysa, M. D., Asano, T. & Noda, S. Realization of dynamic thermal emission control. *Nat. Mater.* **13**, 928–931 (2014).
217. Brar, V. W. et al. Electronic modulation of infrared radiation in graphene plasmonic resonators. *Nat. Commun.* **6**, 7032 (2015).
218. Park, J. et al. Dynamic thermal emission control with InAs-based plasmonic metasurfaces. *Sci. Adv.* **4**, eaat3163 (2018).
219. Thomas, N. H., Sherrott, M. C., Broulliet, J., Atwater, H. A. & Minnich, A. J. Electronic modulation of near-field radiative transfer in graphene field effect heterostructures. *Nano Lett.* **19**, 3898–3904 (2019).
220. Xu, C., Stiubianu, G. T. & Gorodetsky, A. A. Adaptive infrared-reflecting systems inspired by cephalopods. *Science* **359**, 1495–1500 (2018).
221. Mandal, J. et al. $Li_4Ti_5O_{12}$: a visible-to-infrared broadband electrochromic material for optical and thermal management. *Adv. Funct. Mater.* **28**, 1802180 (2018).
222. Moncada-Villa, E., Fernández-Hurtado, V., García-Vidal, F. J., García-Martín, A. & Cuevas, J. C. Magnetic field control of near-field radiative heat transfer and the realization of highly tunable hyperbolic thermal emitters. *Phys. Rev. B* **92**, 125418 (2015).
223. Latella, I. & Ben-Abdallah, P. Giant thermal magnetoresistance in plasmonic structures. *Phys. Rev. Lett.* **118**, 173902 (2017).
224. Ge, L. et al. Magnetically tunable multiband near-field radiative heat transfer between two graphene sheets. *Phys. Rev. B* **100**, 035414 (2019).
225. Coppens, Z. J. & Valentine, J. G. Spatial and temporal modulation of thermal emission. *Adv. Mater.* **29**, 1701275 (2017).
226. Xiao, Y., Charipar, N. A., Salman, J., Piqué, A. & Kats, M. A. Nanosecond mid-infrared pulse generation via modulated thermal emissivity. *Light Sci. Appl.* **8**, 1–8 (2019).
227. Liu, X. & Padilla, W. J. Reconfigurable room temperature metamaterial infrared emitter. *Optica* **4**, 430–433 (2017).
228. Zhang, X. A. et al. Dynamic gating of infrared radiation in a textile. *Science* **363**, 619–623 (2019).
229. Phan, L. et al. Reconfigurable infrared camouflage coatings from a cephalopod protein. *Adv. Mater.* **25**, 5621–5625 (2013).
230. Kats, M. A. et al. Vanadium dioxide as a natural disordered metamaterial: perfect thermal emission and large broadband negative differential thermal emittance. *Phys. Rev. X* **3**, 041004 (2013).
231. van Zwol, P. J., Ranno, L. & Chevrier, J. Tuning near field radiative heat flux through surface excitations with a metal insulator transition. *Phys. Rev. Lett.* **108**, 234301 (2012).
232. Du, K. et al. Control over emissivity of zero-static-power thermal emitters based on phase-changing material GST. *Light Sci. Appl.* **6**, e16194 (2016).
233. Xiao, L. et al. Fast adaptive thermal camouflage based on flexible VO_2/graphene/CNT thin films. *Nano Lett.* **15**, 8365–8370 (2015).
234. Philippe, B. & Biehs, S. Phase-change radiative thermal diode. *Appl. Phys. Lett.* **103**, 191907 (2013).

235. Ito, K., Nishikawa, K., Iizuka, H. & Toshiyoshi, H. Experimental investigation of radiative thermal rectifier using vanadium dioxide. *Appl. Phys. Lett.* **105**, 253503 (2014).
236. Wu et al. Thermal homeostasis using microstructured phase-change materials. *Optica* **4**, 1390–1396 (2017).
237. Ono, Masashi, Chen, K., Li, W. & Fan, S. Self-adaptive radiative cooling based on phase change materials. *Opt. Express* **26**, A777–A787 (2018).
238. Dede, E. M., Nomura, T., Schmalenberg, P. & Lee, J. S. Heat flux cloaking, focusing, and reversal in ultra-thin composites considering conduction–convection effects. *Appl. Phys. Lett.* **103**, 063501 (2013).
239. Prasher, R., Bhattacharya, P. & Phelan, P. E. Brownian-motion-based convective–conductive model for the effective thermal conductivity of nanofluids. *J. Heat Transf.* **128**, 588–595 (2005).
240. Bejan, A. *Convection Heat Transfer* (Wiley, 2013).
241. Guenneau, S. & Puvirajesinghe, T. M. Fick's second law transformed: one path to cloaking in mass diffusion. *J. R. Soc. Interface* **10**, 20130106 (2013).
242. Dai, G., Shang, J. & Huang, J. Theory of transformation thermal convection for creeping flow in porous media: cloaking, concentrating, and camouflage. *Phys. Rev. E* **97**, 022129 (2018).
243. Urzhumov, Y. A. & Smith, D. R. Fluid flow control with transformation media. *Phys. Rev. Lett.* **107**, 074501 (2011).
244. Li, Y. et al. Anti-parity–time symmetry in diffusive systems. *Science* **364**, 170–173 (2019). **This paper provides a non-Hermitian Hamiltonian description of heat transfer**.
245. Cao, P., Li, Y., Peng, Y., Qiu, C.-W. & Zhu, X. High-order exceptional points in diffusive systems: robust APT symmetry against perturbation and phase oscillation at APT symmetry breaking. *ES Energy Env.* **7**, 48–55 (2020).
246. Özdemir, Ş. K., Rotter, S., Nori, F. & Yang, L. Parity–time symmetry and exceptional points in photonics. *Nat. Mater.* **18**, 783–798 (2019).
247. Ye, Z.-Q. & Cao, B.-Y. Nanoscale thermal cloaking in graphene via chemical functionalization. *Phys. Chem. Chem. Phys.* **18**, 32952–32961 (2016).
248. Hu, R. et al. Encrypted thermal printing with regionalization transformation. *Adv. Mater.* **31**, 1807849 (2019).
249. Xu, L. & Huang, J. Metamaterials for manipulating thermal radiation: transparency, cloak, and expander. *Phys. Rev. Appl.* **12**, 044048 (2019).
250. Xu, L., Dai, G. & Huang, J. Transformation multithermotics: controlling radiation and conduction simultaneously. *Phys. Rev. Appl.* **13**, 024063 (2020).
251. Strohm, C., Rikken, G. L. J. A. & Wyder, P. Phenomenological evidence for the phonon Hall effect. *Phys. Rev. Lett.* **95**, 155901 (2005).
252. Zhang, L., Ren, J., Wang, J. S. & Li, B. Topological nature of the phonon Hall effect. *Phys. Rev. Lett.* **105**, 225901 (2010).
253. Ma, G., Xiao, M. & Chan, C. T. Topological phases in acoustic and mechanical systems. *Nat. Rev. Phys.* **1**, 281–294 (2019).
254. Xu, N., Xu, Y. & Zhu, J. Topological insulators for thermoelectrics. *NPJ Quantum Mater.* **2**, 1–9 (2017).
255. Granger, G., Eisenstein, J. P. & Reno, J. L. Observation of chiral heat transport in the quantum Hall regime. *Phys. Rev. Lett.* **102**, 086803 (2009).
256. Onose, Y. et al. Observation of the magnon Hall effect. *Science* **329**, 297–299 (2010).
257. Mochizuki, M. et al. Thermally driven ratchet motion of a skyrmion microcrystal and topological magnon Hall effect. *Nat. Mater.* **13**, 241–246 (2014).
258. Rivas, Ã. & Martin-Delgado, M. A. Topological heat transport and symmetry-protected boson currents. *Sci. Rep.* **7**, 6350 (2017).
259. Lu, L., Joannopoulos, J. D. & Soljačić, M. Topological photonics. *Nat. Photonics* **8**, 821–829 (2014).
260. Ozawa, T. et al. Topological photonics. *Rev. Mod. Phys.* **91**, 015006 (2019).
261. Zhu, L., Guo, Y. & Fan, S. Theory of many-body radiative heat transfer without the constraint of reciprocity. *Phys. Rev. B* **97**, 094302 (2018).
262. Joseph, D. D. & Preziosi, L. Heat waves. *Rev. Mod. Phys.* **61**, 41–73 (1989).
263. Chester, M. Second sound in solids. *Phys. Rev.* **131**, 2013 (1963).
264. Huberman, S. et al. Observation of second sound in graphite at temperatures above 100 K. *Science* **364**, 375–379 (2019).
265. Cepellotti, A. et al. Phonon hydrodynamics in two-dimensional materials. *Nat. Commun.* **6**, 6400 (2015).
266. Lee, S., Broido, D., Esfarjani, K. & Chen, G. Hydrodynamic phonon transport in suspended graphene. *Nat. Commun.* **6**, 6290 (2015).
267. Principi, A., Katsnelson, M. I. & Levchenko, A. Chiral second-sound collective modes at the edge of 2D systems with a nontrivial berry curvature. *Phys. Rev. Lett.* **118**, 036802 (2017).
268. Ruokola, T., Ojanen, T. & Jauho, A. P. Thermal rectification in nonlinear quantum circuits. *Phys. Rev. B* **79**, 144306 (2009).
269. Joulain, K., Drevillon, J., Ezzahri, Y. & Ordonez-Miranda, J. Quantum thermal transistor. *Phys. Rev. Lett.* **116**, 200601 (2016).
270. Scully, M. O., Suhail Zubairy, M., Agarwal, G. S. & Walther, H. Extracting work from a single heat bath via vanishing quantum coherence. *Science* **299**, 862–864 (2003).
271. Roßnagel, J. et al. A single-atom heat engine. *Science* **352**, 325–329 (2016).
272. Koski, J. V., Kutvonen, A., Khaymovich, I. M., Ala-Nissila, T. & Pekola, J. P. On-chip Maxwell's demon as an information-powered refrigerator. *Phys. Rev. Lett.* **115**, 260602 (2015).
273. Gemmer, J., Michel, M. & Mahler, G. *Quantum Thermodynamics: Emergence of Thermodynamic Behavior within Composite Quantum Systems* (Springer, 2009).
274. Brandão, F., Horodecki, M., Ng, N., Oppenheim, J. & Wehner, S. The second laws of quantum thermodynamics. *Proc. Natl Acad. Sci. USA* **112**, 3275–3279 (2015).
275. Micadei, K. et al. Reversing the direction of heat flow using quantum correlations. *Nat. Commun.* **10**, 2456 (2019).
276. Klatzow, J. et al. Experimental demonstration of quantum effects in the operation of microscopic heat engines. *Phys. Rev. Lett.* **122**, 110601 (2019).
277. Ezzahri, Y. & Joulain, K. Vacuum-induced phonon transfer between two solid dielectric materials: Illustrating the case of Casimir force coupling. *Phys. Rev. B* **90**, 115433 (2014).
278. Pendry, J. B., Sasihithlu, K. & Craster, R. V. Phonon-assisted heat transfer between vacuum-separated surfaces. *Phys. Rev. B* **94**, 075414 (2016).
279. Pollack, G. L. Kapitza resistance. *Rev. Mod. Phys.* **41**, 48–81 (1969).
280. Li, B., Lan, J. & Wang, L. Interface thermal resistance between dissimilar anharmonic lattices. *Phys. Rev. Lett.* **95**, 104302 (2005).
281. Swartz, E. T. & Pohl, R. O. Thermal boundary resistance. *Rev. Mod. Phys.* **61**, 605–668 (1989).
282. Monachon, C., Weber, L. & Dames, C. Thermal boundary conductance: a materials science perspective. *Annu. Rev. Mater. Res.* **46**, 433–463 (2016).
283. Giri, A. & Hopkins, P. E. A review of experimental and computational advances in thermal boundary conductance and nanoscale thermal transport across solid interfaces. *Adv. Funct. Mater.* **30**, 1903857 (2020).
284. Slack, G. A. Nonmetallic crystals with high thermal conductivity. *J. Phys. Chem. Solids* **34**, 321–335 (1973).
285. Wei, L., Kuo, P. K., Thomas, R. L., Anthony, T. R. & Banholzer, W. F. Thermal conductivity of isotopically modified single crystal diamond. *Phys. Rev. Lett.* **70**, 3764–3767 (1993).
286. Kang, J. S., Li, M., Wu, H., Nguyen, H. & Hu, Y. Experimental observation of high thermal conductivity in boron arsenide. *Science* **361**, 575–578 (2018).
287. Li, S. et al. High thermal conductivity in cubic boron arsenide crystals. *Science* **361**, 579–581 (2018).
288. Tian, F. et al. Unusual high thermal conductivity in boron arsenide bulk crystals. *Science* **361**, 582–585 (2018).
289. Chen, K. et al. Ultrahigh thermal conductivity in isotope-enriched cubic boron nitride. *Science* **367**, 555–559 (2020).
290. Onsager, L. Reciprocal relations in irreversible processes. I. *Phys. Rev.* **37**, 405–426 (1931).
291. Katsura, H., Nagaosa, N. & Lee, P. A. Theory of the thermal Hall effect in quantum magnets. *Phys. Rev. Lett.* **104**, 066403 (2010).
292. Gaussorgues, G. & Chomet, S. *Infrared Thermography* (Springer, 1994).
293. Dede, E. M., Schmalenberg, P., Wang, C.-M., Zhou, F. & Nomura, T. Collection of low-grade waste heat for enhanced energy harvesting. *AIP Adv.* **6**, 055113 (2016).
294. Joulain, K., Mulet, J., Marquier, F., Carminati, R. & Greffet, J. Surface electromagnetic waves thermally excited: radiative heat transfer, coherence properties and Casimir forces revisited in the near field. *Surf. Sci. Rep.* **57**, 59–112 (2005).

Acknowledgements
C.-W.Q. acknowledges support from the Ministry of Education, Singapore (grant no. R-263-000-E19-114). W.L. and S.F. acknowledge support by the US Department of Energy (grant no. DE-FG02-07ER46426). W.L. acknowledges discussions with W. Jin and L. Fan.

Author contributions
C.W., Y.L., B.L., W.L. and S.F. discussed the content of the Review. Y.L, W.L, T.H. and X.Z. wrote the Review. All authors reviewed and edited the manuscript before submission.

Competing interests
The authors declare no competing interests.

Publisher's note
Springer Nature remains neutral with regard to jurisdictional claims in published maps and institutional affiliations.